

Probing CP Violation in Dark Sector through the Electron Electric Dipole Moment

 Jia Liu ^{*1,2}, Yuichiro Nakai ^{†3,4},

Yoshihiro Shigekami ^{‡3,4}, and Muyuan Song ^{§2,1}

¹ *School of Physics and State Key Laboratory of Nuclear Physics and Technology,
Peking University, Beijing 100871, China*

² *Center for High Energy Physics, Peking University, Beijing 100871, China*

³ *Tsung-Dao Lee Institute, Shanghai Jiao Tong University,
520 Shengrong Road, Shanghai 201210, China*

⁴ *School of Physics and Astronomy, Shanghai Jiao Tong University,
800 Dongchuan Road, Shanghai 200240, China*

Abstract

The Two Higgs Doublet Model (2HDM) stands as a promising framework for exploring physics beyond the Standard Model (SM). Within this context, we explore the possibility that the two Higgs doublets may serve as a window into CP-violating dark sectors, neutral under the SM gauge groups. Specifically, our focus is on investigating the electric dipole moment (EDM) of the electron, generated solely by CP violation in the dark sector. We present a general formula for the electron EDM, without specifying the structure of the dark sectors, and discuss the current constraints on various dark sector models. It is noteworthy that even in the case of a CP-conserving 2HDM, the resulting electron EDM is capable of reaching the current experimental limit, with CP violation arising exclusively from the dark sectors. Furthermore, we introduce a heavy dark sector (HDS) approximation for the analytic calculation of the EDM, assuming that the dark sector particles are much heavier than the physical states in the 2HDM. This approximation yields simplified analytic results that are consistent with the full numerical calculations.

*jialiu@pku.edu.cn

†ynakai@sjtu.edu.cn

‡shigekami@sjtu.edu.cn

§muyuansong@pku.edu.cn

Contents

1	Introduction	3
2	The framework	4
2.1	Two Higgs Doublet Model	4
2.2	2HDM portal to the dark sector	7
3	EDMs from general dark sector	7
3.1	Current limits on EDMs	8
3.2	The CP-violating diagrams	9
3.3	The four-fermion diagram	10
3.4	The Barr-Zee diagrams	11
3.4.1	The heavy dark sector limit	13
4	Numerical analysis for benchmark models	15
4.1	Scalar dark sector model	15
4.1.1	Numerical results	20
4.1.2	Discussion on the HDS approximation	22
4.2	Fermion dark sector model	24
4.2.1	Numerical results	28
4.2.2	Discussion on the HDS approximation	29
5	Conclusion	30
A	The 2HDM	31
B	Potential analysis for the fermion dark sector model	32
C	Rephasing-invariant CP-violating phases	34
C.1	CPV phases in the scalar dark sector model	35
C.2	CPV phases in the fermion dark sector model	35
D	Details of calculations	36
D.1	General dark sector	36
D.2	Heavy dark sector	38
D.3	Decomposed expressions for the electron EDM	39

1 Introduction

Identifying the structure of the Higgs sector to spontaneously break the electroweak symmetry is one of the most important missions in modern particle physics. Despite that the discovery of the Higgs boson at the Large Hadron Collider (LHC) [1,2] largely advances our understanding of the Higgs sector, the current experimental data still allow a lot of freedom for its structure. Among others, two Higgs doublet models (2HDMs) [3] are classified into the simplest and viable extensions of the Standard Model (SM) Higgs sector (see *e.g.* ref. [4] for a review). 2HDMs are motivated by various phenomenological reasons. One of them is supersymmetry, which requires two Higgs doublets to give masses to both up-type and down-type fermions [5–8]. Another motivation is dark matter (DM), which can be provided by a stable neutral scalar in some versions of 2HDMs, such as the inert doublet model [9–14]. Therefore, the paradigm of 2HDMs has been considered one of the top candidates of physics beyond SM. In the present paper, we point out a new interesting feature of 2HDMs: two Higgs doublets become a window with a good view of CP-violating dark sectors that are neutral under the SM gauge groups but interact with SM particles through two Higgs doublet portal couplings.

Exploration of dark sector models has received a lot of attention recently. In particular, if a dark sector contains a new source of CP violation, it may be able to address the matter-antimatter asymmetry of the Universe. In fact, refs. [15,16] have demonstrated a connection between CP violation in a dark sector and electroweak baryogenesis, which is responsible for the observed baryon asymmetry during the electroweak phase transition (EWPT). While new light particles in a dark sector are often probed by high-intensity accelerator-based experiments, a CP-violating dark sector may generate electric dipole moments (EDMs) of nucleons, atoms, and molecules that are precisely measured. Among others, the measurement of the electron EDM is fascinating. The recent results of the ACME [17] and JILA [18,19] experiments have reached $\mathcal{O}(10^{-29} - 10^{-30})$ ecm. Since the electron EDM is immune to QCD effects and its precise calculation is possible, it seems to provide a sensitive probe of a CP-violating dark sector. The authors of ref. [20] have initiated to study of this issue by considering various dark sectors feebly interacting with the SM sector. They found that the effect of dark sector CP violation appears only from higher loops and is too tiny to be observed unless a neutrino portal coupling contains a nonzero complex phase. Ref. [21] has extended the Higgs sector by a complex singlet coupling to a dark sector fermion. The authors showed that such a complex singlet extension does not generate the electron EDM up to at least the two-loop level. Moreover, various researchers have explored the implications of the new dark gauge symmetry coupled with the scalar, generating CP-violation at two-loop levels as well [22]. This implies that EDM originating from the dark sector can be either highly suppressed at

higher loops or, if present at the tree level, plays a vital role in understanding the CP violation.

In the present paper, we explore the effect of dark sector CP violation within the framework of 2HDMs and calculate molecule EDMs that constrain the electron EDM.¹ A new CP-violating phase, which can be $\mathcal{O}(1)$, exists in an interaction involving dark sector particles, while the ordinary 2HDM sector does not contain CP violation. We find that the produced electron EDM reaches the current experimental limit in some parameter space. The 2HDM portal enhances the sensitivity of the electron EDM to a CP-violating dark sector.

The rest of the paper is organized as follows. In section 2, we introduce our setup. Section 3 then presents a general formula for the electron EDM without specifying the structure of a dark sector. To discuss the current constraints numerically, we specify the dark sector structure and consider two cases of a dark complex scalar and a dark vector-like fermion in section 4. Section 5 is devoted to conclusions and discussions. Some calculational details are summarized in appendices.

2 The framework

Let us start with an overview of the features of our CP-conserving 2HDMs and CP-violating dark sectors under consideration in the present paper. The 2HDM is a well-studied case of physics beyond the SM, involving an extra Higgs doublet scalar field. Here, our objective is to provide a brief description of the relevant physical modes and interactions. More details are summarized in appendix A. While the current section does not specify a concrete dark sector model, dark sector CP violation will be encoded through a (radiatively generated) mixing term between CP-even and CP-odd scalars of the 2HDM.

2.1 Two Higgs Doublet Model

The potential of two Higgs doublets $H_{1,2}$ can be expressed as

$$V_H = \sum_{i=1,2} \left[m_i^2 H_i^\dagger H_i + \frac{\lambda_i}{2} \left(H_i^\dagger H_i \right)^2 \right] + \lambda_3 \left(H_1^\dagger H_1 \right) \left(H_2^\dagger H_2 \right) + \lambda_4 \left(H_1^\dagger H_2 \right) \left(H_2^\dagger H_1 \right) + \left[-m_{12}^2 H_1^\dagger H_2 + \frac{\lambda_5}{2} \left(H_1^\dagger H_2 \right)^2 + \text{h.c.} \right], \quad (2.1)$$

where m_{12}^2 and λ_5 are generally complex, while the other parameters are real. By field redefinition of either H_1 or H_2 , we can set m_{12}^2 or λ_5 to be real, while $\arg[\lambda_5^*(m_{12}^2)^2]$

¹Ref. [23] has discussed a similar setup in a different context and studied a dark sector contribution to anomalous gauge couplings.

Type	Yukawa terms
Type-I ($d_R : +, e_R : +$)	$-Y_u^{(2)}\overline{Q_L}\widetilde{H}_2u_R - Y_d^{(2)}\overline{Q_L}H_2d_R - Y_e^{(2)}\overline{L_L}H_2e_R + \text{h.c.}$
Type-II ($d_R : -, e_R : -$)	$-Y_u^{(2)}\overline{Q_L}\widetilde{H}_2u_R - Y_d^{(1)}\overline{Q_L}H_1d_R - Y_e^{(1)}\overline{L_L}H_1e_R + \text{h.c.}$
Type-X ($d_R : +, e_R : -$)	$-Y_u^{(2)}\overline{Q_L}\widetilde{H}_2u_R - Y_d^{(2)}\overline{Q_L}H_2d_R - Y_e^{(1)}\overline{L_L}H_1e_R + \text{h.c.}$
Type-Y ($d_R : -, e_R : +$)	$-Y_u^{(2)}\overline{Q_L}\widetilde{H}_2u_R - Y_d^{(1)}\overline{Q_L}H_1d_R - Y_e^{(2)}\overline{L_L}H_2e_R + \text{h.c.}$

Table 1: The four types of Yukawa couplings in the 2HDM, showing the Z_2 charges of d_R and e_R along with the type names in the first column and the allowed Yukawa couplings in the second column. Note that Q_L and L_L are assumed to be even under the Z_2 .

remains invariant. This phase is severely constrained by the electron EDM measurement, as previously studied in refs. [24–32]. Since our focus is on dark sector CP violation and how it is transferred into the 2HDM sector, we assume that the pure 2HDM sector is CP-conserving, $\arg[\lambda_5^*(m_{12}^2)^2] = 0$, and both λ_5 and m_{12}^2 are real². The two $SU(2)_L$ doublets $H_{1,2}$ are parametrized as

$$H_i = \begin{pmatrix} H_i^+ \\ (v_i + H_i^0 + iA_i^0)/\sqrt{2} \end{pmatrix} \quad (i = 1, 2). \quad (2.2)$$

Here, v_1 and v_2 are nonzero vacuum expectation values (VEVs) for the neutral components of H_1 and H_2 , respectively. They are related by $v_1^2 + v_2^2 = v_{\text{SM}}^2 = (246.22 \text{ GeV})^2$. We define their ratio as

$$\tan \beta \equiv \frac{v_2}{v_1}. \quad (2.3)$$

Upon diagonalizing the mass matrices derived from the scalar potential in Eq. (2.1), we obtain the mass eigenstates for the neutral scalars:

$$H_1^0 = H^0 c_\alpha - h^0 s_\alpha, \quad H_2^0 = H^0 s_\alpha + h^0 c_\alpha, \quad (2.4)$$

$$A_1^0 = G^0 c_\beta - A^0 s_\beta, \quad A_2^0 = G^0 s_\beta + A^0 c_\beta, \quad (2.5)$$

with mixing angle α whose expression is provided in Eq. (A.11). Here, G^0 represents the Nambu-Goldstone (NG) field, while h^0 and H^0 denote the two CP-even scalars, with the former being the SM Higgs, and A^0 represents the CP-odd heavy scalar.

The Yukawa couplings for SM fermions in the 2HDM are represented by the following Lagrangian term:

$$\mathcal{L}_{\text{Yuk}} = -Y_u^{(i)}\overline{Q_L}\widetilde{H}_i u_R - Y_d^{(i)}\overline{Q_L}H_i d_R - Y_e^{(i)}\overline{L_L}H_i e_R + \text{h.c.}, \quad (2.6)$$

²Even we consider the CP-conserving 2HDM, CP is not a symmetry of our study, because of the CP violation in the dark sector.

	ξ_h^u	ξ_H^u	ξ_A^u	ξ_h^d	ξ_H^d	ξ_A^d	ξ_h^e	ξ_H^e	ξ_A^e
Type-I	c_α/s_β	s_α/s_β	$\cot \beta$	c_α/s_β	s_α/s_β	$-\cot \beta$	c_α/s_β	s_α/s_β	$-\cot \beta$
Type-II	c_α/s_β	s_α/s_β	$\cot \beta$	$-s_\alpha/c_\beta$	c_α/c_β	$\tan \beta$	$-s_\alpha/c_\beta$	c_α/c_β	$\tan \beta$
Type-X	c_α/s_β	s_α/s_β	$\cot \beta$	c_α/s_β	s_α/s_β	$-\cot \beta$	$-s_\alpha/c_\beta$	c_α/c_β	$\tan \beta$
Type-Y	c_α/s_β	s_α/s_β	$\cot \beta$	$-s_\alpha/c_\beta$	c_α/c_β	$\tan \beta$	c_α/s_β	s_α/s_β	$-\cot \beta$

Table 2: The coefficients between SM fermions and physical neutral scalars.

where $\tilde{H}_i = i\sigma_2 H_i^*$, Q_L and L_L denote the left-handed $SU(2)_L$ doublet quark and lepton, and u_R , d_R and e_R are the right-handed $SU(2)_L$ singlet up-type quark, down-type quark and charged lepton. In general, there are Yukawa couplings associated with both H_1 and H_2 for each SM fermion. However, including both Yukawa couplings easily leads to dangerous flavor-changing neutral current (FCNC) processes. To avoid such a situation, one can assume different symmetry properties for H_1 and H_2 [33]. For example, H_1 behaves as odd while H_2 as even under a discrete Z_2 symmetry.³ Without loss of generality, one can select a scenario in which $\overline{Q}_L u_R$ couples exclusively to H_2 . Then, there are four types of Yukawa coupling arrangements, namely Type-I, II, X, and Y, depending on the charges of d_R and e_R , which are summarized in Table 1. Due to the mixings in Eqs. (2.4) and (2.5), the Yukawa interactions between the SM fermions and the physical neutral scalars are given by

$$\mathcal{L}_{\text{Yuk}} \supset - \sum_{f=u,d,e} \frac{m_f}{v_{\text{SM}}} \left(\xi_h^f \bar{f} f h^0 + \xi_H^f \bar{f} f H^0 - \xi_A^f \bar{f} i \gamma^5 f A^0 \right), \quad (2.7)$$

where m_f is the SM fermion mass, and the coefficients $\xi_{h,H,A}^f$ are summarized in Table 2. It is notable that the lepton couplings to the heavy scalars are significantly enhanced by a large $\tan \beta$ for Type-II and Type-X 2HDMs, leading to a larger effect on the electron EDM.

Due to the additional Higgs doublet, the W boson couplings to CP-even scalars are modified as

$$\mathcal{L} \supset \frac{2m_W^2}{v_{\text{SM}}} s_{\beta-\alpha} W_\mu^+ W^{-\mu} h^0 + \frac{2m_W^2}{v_{\text{SM}}} c_{\beta-\alpha} W_\mu^+ W^{-\mu} H^0. \quad (2.8)$$

Note that if the model does not mix between CP-even and CP-odd scalars, there is no W boson coupling to the CP-odd scalar, A^0 [34].

³Under the Z_2 symmetry, the scalar potential term $m_{12}^2 H_1^\dagger H_2$ in Eq. (2.1) can be considered as a soft Z_2 breaking term.

2.2 2HDM portal to the dark sector

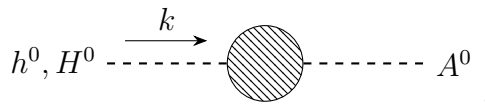
To couple the 2HDM to a dark sector, which is neutral under the SM gauge symmetry, we make the following assumptions:

- (i) The dark sector incorporates physical CP phase(s), and it does not contain any new scalar field that acquires a nonzero VEV.
- (ii) New scalar potential terms that couple $H_{1,2}$ to the dark sector are expressed as

$$V_{HO} = \lambda_{ij} H_i^\dagger H_j \mathcal{O}_{ij}^D + \text{h.c.}, \quad (2.9)$$

where \mathcal{O}_{ij}^D represents operators composed of dark sector fields.

The assumption (i) implies the absence of tree-level mass mixing between CP-even and CP-odd scalars in $H_{1,2}$. Loop corrections through the interactions (2.9) generate effective mixing terms for those scalars:



$$h^0, H^0 \text{ --- } \text{blob} \text{ --- } A^0, \quad (2.10)$$

where the gray shaded blob represents loops of dark sector particles. Nonzero mass mixing between CP-even (h^0, H^0) and CP-odd (A^0) scalars in the 2HDM is induced by dark sector CP violation.

We have comment on a renormalization group (RG) running of couplings in 2HDM sector. When we consider a UV complete model that incorporates our dark sector, the RG running induces a phase for λ_5 as well as m_{12}^2 , due to the coupling between 2HDM and dark sectors in Eq. (2.9). In addition, there is the possibility of generating terms such as $\lambda_6(H_1^\dagger H_1)(H_1^\dagger H_2) + \lambda_7(H_2^\dagger H_2)(H_1^\dagger H_2) + \text{h.c.}$ through the RG running, which have complex parameters of $\lambda_{6,7}$. These terms and λ_5 are additional sources of CP violation, inducing a CP-violating nature in our 2HDM sector where CP-even and CP-odd scalars mix. As mentioned in section 2.1, a CP-violating 2HDM is severely constrained by the bound on d_e , and the current focus is electron EDM prediction from dark sector CP violation. Therefore, we specifically consider a scenario in which the phases of $\lambda_{5,6,7}$ induced by the RG running are sufficiently small. This ensures that contributions from these CP phases to the electron EDM are sub-dominant, allowing our EDM prediction to be predominantly influenced by CP violation in the dark sector. The details of effect of this RG running will be performed in the future work.

3 EDMs from general dark sector

We now summarize the current experimental limits on molecule EDMs which constrain the electron EDM, and derive analytical expressions for dark sector contributions to the

EDMs without specifying the detailed structure of the dark sector. As mentioned in the previous section, the mixing between CP-even and CP-odd scalars is induced via loops of CP-violating dark sector particles.

3.1 Current limits on EDMs

Measuring EDMs of leptons, nucleons, atoms, and molecules stands as one of the most sensitive probes of new physics with CP violation, and numerous experiments set upper limits on their magnitudes [17, 18, 35, 36], which put stringent constraints on models incorporating CP violation, such as the complex 2HDM and supersymmetry (see e.g. refs. [37, 38]). For an in-depth understanding of EDMs and their measurement techniques, along with theoretical aspects, one can refer to comprehensive reviews such as refs. [39–41].

One intriguing approach in EDM experiments is to utilize paramagnetic atoms or molecules. A particularly stringent constraint on the electron EDM from this type of experiment was reported by the ACME collaboration before 2022 [17]. They conducted a measurement on the EDM of the paramagnetic ThO molecule, establishing an upper bound of $|d_{\text{ThO}}| < 1.1 \times 10^{-29} e \text{ cm}$ at 90% confidence level (CL). For paramagnetic molecules, the EDM measurement offers sensitivity not only to the electron EDM d_e but also to the CP-odd electron-nucleon interaction C_S . The relevant dimension-five and dimension-six operators are described by the following Lagrangian:

$$\mathcal{L}_{\text{EDM},eN} \supset -\frac{i}{2} d_e \bar{e} \sigma^{\mu\nu} \gamma^5 e F_{\mu\nu} - C_S \bar{e} i \gamma^5 e \bar{N} N, \quad (3.1)$$

where $\sigma^{\mu\nu} = \frac{i}{2} [\gamma^\mu, \gamma^\nu]$, and N represents the nucleon. These CP-violating interactions contribute to the EDM of the paramagnetic molecule, and the bound from the ACME collaboration is expressed as [17]

$$|d_e + k_{\text{ThO}} C_S| < 1.1 \times 10^{-29} e \text{ cm}, \quad (3.2)$$

with $k_{\text{ThO}} \simeq 1.8 \times 10^{-15} \text{ GeV}^2 e \text{ cm}$, where we have used $\mathcal{E}_{\text{eff}}^{\text{ThO}} \approx 78 \text{ GVcm}^{-1}$ for the effective electric field and $W_S^{\text{ThO}} = -282 \text{ kHz} \times h$ for the molecule specific constant.

Towards the end of 2022, the JILA experiments presented a new upper bound on the electron EDM, utilizing the HfF⁺ molecule ion [18, 19]. The result is expressed as $|d_{\text{HfF}^+}| < 4.1 \times 10^{-30} e \text{ cm}$ at 90% CL, which can be interpreted as

$$|d_e + k_{\text{HfF}^+} C_S| < 4.1 \times 10^{-30} e \text{ cm}, \quad (3.3)$$

with $k_{\text{HfF}^+} \simeq 1.1 \times 10^{-15} \text{ GeV}^2 e \text{ cm}$, where we have used $\mathcal{E}_{\text{eff}}^{\text{HfF}^+} \approx 23 \text{ GVcm}^{-1}$ for the effective electric field and $W_S^{\text{HfF}^+} = -51 \text{ kHz} \times h$ for the molecule specific constant.

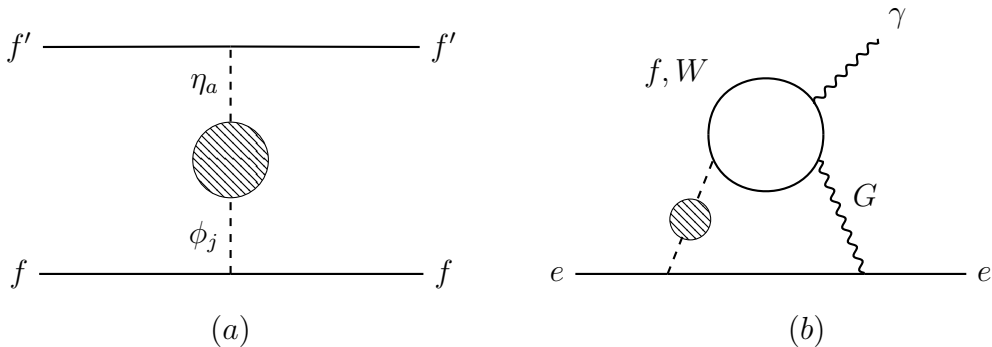


Figure 1: The two diagrams relevant to the CP-violating Lagrangian in Eq. (3.1). *Left:* The four-fermion operators mediated by the scalars. *Right:* The Barr-Zee diagram contributing to the electron EDM, with G denoting the photon or Z boson. In both diagrams, the scalar lines represent the CP-even scalars ϕ_j or CP-odd scalars η_a , and the gray shaded blob symbolizes the effective mixing between ϕ_j and η_a arising from the CP-violating dark sector contribution, which corresponds to $F_{\text{DS}}^{\phi_j \eta_a}(k^2, M^2)$ in Eq. (3.6).

In addition to EDMs of paramagnetic molecules, there are experiments to measure EDMs of diamagnetic atoms, such as the mercury EDM [42] and the neutron EDM [36]. These experiments, in principle, can impose constraints on the 2HDM or supersymmetry, and the details can be found in refs. [43, 44]. However, upon careful examination, we have verified that the electron EDM constraint in the JILA experiment is considerably stronger than the bounds stemming from the other EDM experiments. Consequently, we focus on the constraint obtained by the JILA experiment in the following discussion.

3.2 The CP-violating diagrams

Let us now consider dark sector contributions to the CP-violating Lagrangian in Eq. (3.1). The relevant contributions are shown in Fig. 1. The left diagram leads to the four-fermion operator $C_S \bar{e} i \gamma^5 e \bar{N} N$, while the right corresponds to the Barr-Zee (BZ) diagram that results in the electron EDM operator $d_e \bar{e} \sigma^{\mu\nu} \gamma^5 e F_{\mu\nu}$ [45]. We can also consider one-loop diagrams induced by loops of neutral scalars, but when compared with the diagrams (a), (b) in Fig. 1, these one-loop diagrams are suppressed by the cubic power of the electron mass m_e^3 : one arises from a chirality flip on the electron line and the others stem from electron-neutral scalar couplings. Therefore, for the current study, we can neglect these one-loop diagrams.

We keep our calculation as general as possible by incorporating a general CP-violating dark sector contribution into the two diagrams of Fig. 1 as propagator corrections. Moreover, we consider a general scalar model with N_E CP-even and N_O CP-odd neutral scalars contributing to the diagrams, denoted as ϕ_j and η_a , respectively. For example, the 2HDM can be identified with $(N_E, N_O) = (2, 2)$ and $(\phi_1, \phi_2, \eta_1, \eta_2) = (h^0, H^0, G^0, A^0)$.

Note that we assume η_1 always represents the NG field G^0 , and thus, the sum of the index a should start from 2 for η_a scalars. ϕ_j and η_a are considered as mass eigenstates, and hence, masses for these scalars are described as

$$V_{\text{scl}} \supset \sum_{j=1}^{N_E} m_{\phi_j}^2 \phi_j^2 + \sum_{a=2}^{N_O} m_{\eta_a}^2 \eta_a^2. \quad (3.4)$$

Here, we assume $m_{\phi_1}^2 < m_{\phi_2}^2 < \dots < m_{\phi_{N_E}}^2$ and $m_{\eta_2}^2 < m_{\eta_3}^2 < \dots < m_{\eta_{N_O}}^2$.

The neutral scalars ϕ_j, η_a couple to the SM fermions through the Yukawa terms in the 2HDM. In addition, CP-even scalars also couple to the W boson. We then have the following Lagrangian terms:

$$\mathcal{L} \supset - \sum_{j=1}^{N_E} \sum_{a=2}^{N_O} \sum_{f=u,d,e} \frac{m_f}{v_{\text{SM}}} \left(\xi_{\phi_j}^f \bar{f} f \phi_j - \xi_{\eta_a}^f \bar{f} i \gamma^5 f \eta_a \right) + \sum_{j=1}^{N_E} \frac{2m_W^2}{v_{\text{SM}}} \xi_{\phi_j}^W W_\mu^+ W^{-\mu} \phi_j, \quad (3.5)$$

where ξ_{ϕ_j, η_a}^f and $\xi_{\phi_j}^W$ are related to $\tan \beta$ and mixing angles for ϕ_j and η_a in the visible sector (for the 2HDM, see Table 2 and Eq. (2.8)). Note that there is no coupling between a CP-odd scalar and the W boson because our assumption forbids any tree-level mixing between CP-even and CP-odd scalars in the visible sector. Furthermore, since we do not extend the fermion and gauge sectors, couplings among these sectors are unchanged from the SM ones. Finally, we have the effective mixing between ϕ_j and η_a , which is generated in the same manner as in Eq. (2.10). In our analytical calculation, we define its mixing as the following term in the effective Lagrangian:

$$\mathcal{L}_{\text{eff}} \supset F_{\text{DS}}^{\phi_j \eta_a}(k^2, M^2) \phi_j \eta_a, \quad (3.6)$$

where k is four-momentum passing through this effective mixing, and M is a typical mass scale of a dark sector. The gray shaded blobs in Fig. 1 correspond to $F_{\text{DS}}^{\phi_j \eta_a}(k^2, M^2)$.

3.3 The four-fermion diagram

In contrast to the nucleon operator in Eq. (3.1), we introduce a new four-fermion operator at the quark level,

$$\mathcal{L}_{4\text{-fermi}} = C_{ff'} (\bar{f} f) (\bar{f}' i \gamma^5 f'). \quad (3.7)$$

The coefficient $C_{ff'}$ stemming from the diagram (a) can be readily calculated. Moreover, we can set the momentum of the scalar to be zero for the current purpose, i.e., $F_{\text{DS}}^{\phi_j \eta_a}(k^2, M^2) = F_{\text{DS}}^{\phi_j \eta_a}(0, M^2)$. Consequently, we obtain

$$C_{ff'} = \frac{m_f m_{f'}}{v_{\text{SM}}^2} \sum_{j=1}^{N_E} \sum_{a=2}^{N_O} \frac{\xi_{\phi_j}^f}{m_{\phi_j}^2} \frac{\xi_{\eta_a}^{f'}}{m_{\eta_a}^2} F_{\text{DS}}^{\phi_j \eta_a}(0, M^2), \quad (3.8)$$

	$\Phi = \phi_j$	$\Phi = \eta_a$		$G = Z$	$G = \gamma$
$g_{f\Phi}^S$	$-\frac{m_f}{v_{\text{SM}}}\xi_{\phi_j}^f$	0	g_{eG}^V	$\frac{g}{\cos\theta_W}\left(\frac{1}{2}T_3^f - Q_f\sin^2\theta_W\right)$	eQ_f
$g_{f\Phi}^P$	0	$+\frac{m_f}{v_{\text{SM}}}\xi_{\eta_a}^f$	g_{eG}^A	$-\frac{g}{2\cos\theta_W}T_3^f$	0

Table 3: Couplings defined in Eq. (3.11). Here, g denotes the gauge coupling of $SU(2)_L$, θ_W is the weak mixing angle, $e = g\sin\theta_W$ is the electromagnetic coupling, $T_3^f = +1/2(-1/2)$ for $f = u(d, e)$, and Q_f is the electric charge of f .

where $\xi_{\phi_j}^f$ and $\xi_{\eta_a}^{f'}$ are defined in Eq. (3.5).

The $C_{ff'}$ term contributes to C_S in Eq. (3.1). The coefficient of the electron-quark interaction C_{qe} leads to

$$C_S \approx \sum_q C_{qe} \langle N | \bar{q}q | N \rangle \approx C_{ue} \frac{16 \text{ MeV}}{m_u} + C_{de} \frac{29 \text{ MeV}}{m_d} + C_{se} \frac{49 \text{ MeV}}{m_s} \\ + C_{ce} \frac{76 \text{ MeV}}{m_c} + C_{be} \frac{74 \text{ MeV}}{m_b} + C_{te} \frac{77 \text{ MeV}}{m_t}, \quad (3.9)$$

where numerators arise from the matrix elements given in refs. [43, 46],

$$(m_u + m_d) \langle N | \bar{u}u + \bar{d}d | N \rangle \simeq 90 \text{ MeV}, \quad \langle N | \bar{u}u - \bar{d}d | N \rangle \simeq 0, \quad m_s \langle N | \bar{s}s | N \rangle \simeq 49 \text{ MeV}, \\ m_c \langle N | \bar{c}c | N \rangle \simeq 76 \text{ MeV}, \quad m_b \langle N | \bar{b}b | N \rangle \simeq 74 \text{ MeV}, \quad m_t \langle N | \bar{t}t | N \rangle \simeq 77 \text{ MeV}, \quad (3.10)$$

with $m_u/m_d \simeq 0.55$.

3.4 The Barr-Zee diagrams

To calculate the BZ diagram in Fig. 1, it is important to handle the momentum in $F_{\text{DS}}^{\phi_j\eta_a}$ with care, as it is integrated as the outer loop momentum in the BZ diagram. Additionally, since we have not specified our dark sector at this stage, we cannot have any explicit formula for $F_{\text{DS}}^{\phi_j\eta_a}$. Therefore, we present the general result before the loop momentum integration. Before the calculation, we define the relevant couplings for SM fermions as

$$\mathcal{L} \supset \bar{f} (g_{f\Phi}^S + ig_{f\Phi}^P \gamma^5) f \Phi + \bar{f} (g_{fG}^V \gamma^\mu + g_{fG}^A \gamma^\mu \gamma^5) f G_\mu, \quad (3.11)$$

where Φ and G_μ denote the neutral scalars (ϕ_j, η_a) and neutral gauge bosons (Z_μ, A_μ), respectively. Comparing with Eq. (3.5), $g_{f\Phi}^{S,P}$ are related to ξ_{ϕ_j, η_a}^f , and $g_{fG}^{V,A}$ are the usual gauge boson couplings in the SM, as summarized in Table 3.

The relevant sub-diagrams for the BZ diagrams are shown in Fig. 2.⁴ The top panel

⁴The other contributions are mainly coming from diagrams with the charged scalar. As studied in refs. [47, 48], these contributions are sub-dominant, especially in large $\tan\beta$ case. Therefore, we simply ignore its contributions in our work.

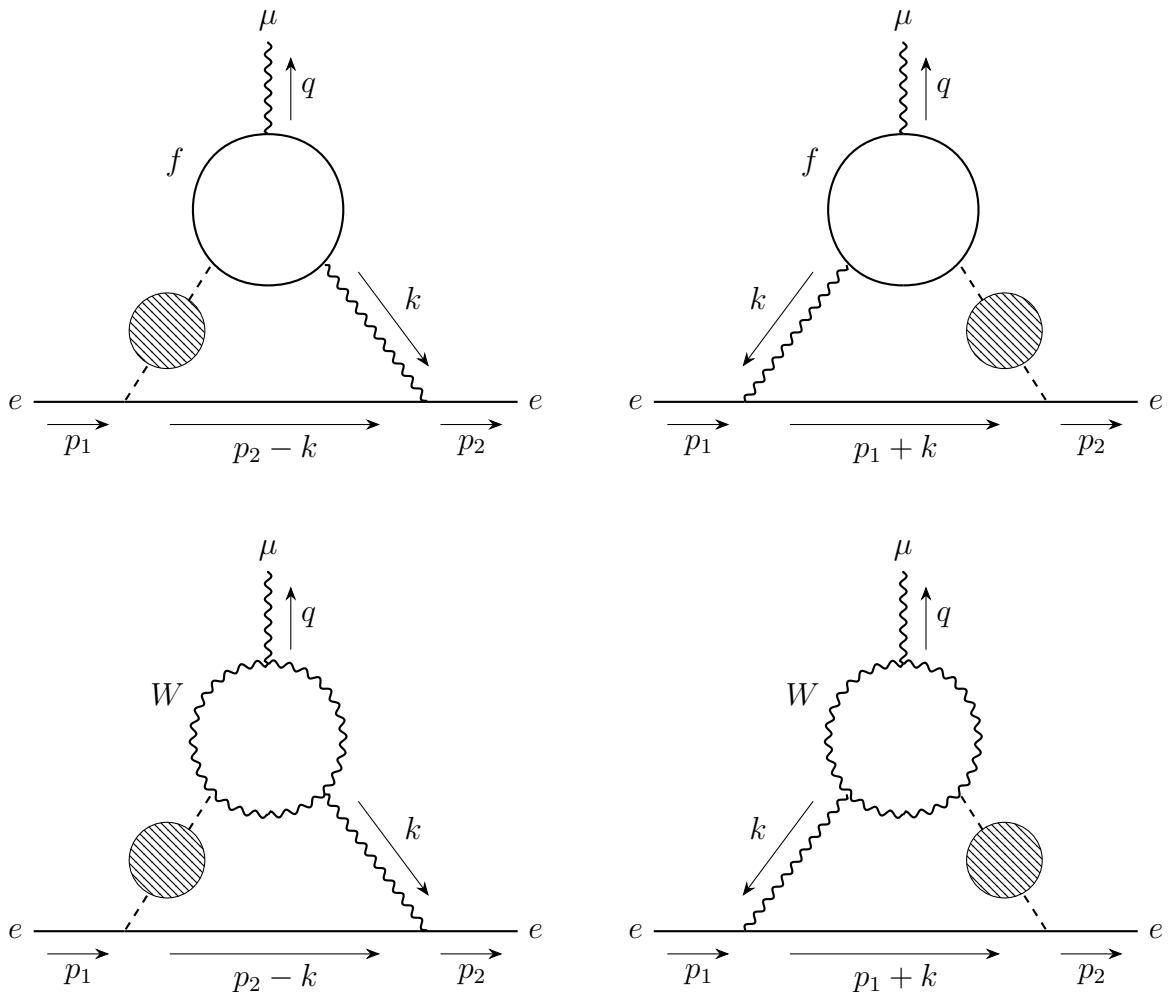


Figure 2: Focused BZ type diagrams with fermion (top diagrams) and W boson (bottom diagrams) loops.

diagrams feature a fermion inner loop, while the bottom panel diagrams have the W boson in the inner loop. In our calculation, we adopt the Feynman-'t Hooft gauge for the W boson propagator and utilize the results from ref. [47]. In general, for W boson contributions to the electron EDM, careful consideration of gauge dependence is necessary, as the diagrams shown in Fig. 2 alone do not yield a gauge-independent result. A comprehensive gauge-independent analysis of the BZ diagrams with W bosons was conducted in ref. [48]. Although numerous diagrams warrant consideration for gauge independence, we focus solely on the diagrams presented in Fig. 2. This is because these diagrams already encompass the leading contributions among the W boson loop diagrams in the Feynman-'t Hooft gauge.

The sum of four diagrams in Fig. 2 leads to a general result of the electron EDM as

$$d_e = \sum_f d_e^f + d_e^W, \quad (3.12)$$

$$\begin{aligned}
d_e^{f,W} &= \sum_{j=1}^{N_E} \sum_{a=2}^{N_O} \int_x \int_y \int_k \frac{F_{\text{DS}}^{\phi_j \eta_a}((k+q)^2, M^2)}{(k^2 - \Delta_{f,W})(k^2 - m_G^2)(k^2 + 2k \cdot q - m_{\phi_j}^2)(k^2 + 2k \cdot q - m_{\eta_a}^2)} \\
&\times \sum_{\Phi=\phi_j, \eta_a} \left(\frac{A_{\alpha\beta}^{L, \Phi(f,W)} k^\alpha k^\beta + B_\alpha^{L, \Phi(f,W)} k^\alpha}{k^2 - 2k \cdot p_2} + \frac{A_{\alpha\beta}^{R, \Phi(f,W)} k^\alpha k^\beta + B_\alpha^{R, \Phi(f,W)} k^\alpha}{k^2 + 2k \cdot p_1} \right), \tag{3.13}
\end{aligned}$$

where we have used $p_{1,2}^2 = m_e^2$ for the outer electron lines, $q = p_1 - p_2$ represents the four-momentum of the external photon, and $\Delta_{f,W}$ is defined as

$$\Delta_{f,W} \equiv \frac{m_{f,W}^2}{x(1-x)} - \frac{2y}{1-x} k \cdot q. \tag{3.14}$$

In addition, we have defined a shorthand notation for each integral as

$$\int_x \equiv \int_0^1 dx \frac{1}{x(1-x)}, \quad \int_y \equiv \int_0^{1-x} dy, \quad \int_k \equiv \int \frac{d^4 k}{(2\pi)^4}, \tag{3.15}$$

where x and y are Feynman parameters arising from the inner loop. The terms $A_{\alpha\beta}^{L, \Phi(f,W)}$, $A_{\alpha\beta}^{R, \Phi(f,W)}$, $B_\alpha^{L, \Phi(f,W)}$, and $B_\alpha^{R, \Phi(f,W)}$ represent the relevant contributions to the electron EDM from fermion and W boson loop diagrams. The explicit expressions for these terms are summarized in appendix D.1.

The expressions in Eq. (3.13) are general and applicable to any dark sector models. Before delving into the numerical calculation, we emphasize the following points:

- (1) The momenta $p_{1,2}$ correspond to the external electron momenta. Thus, terms such as $k \cdot p_i$ and $k \cdot q$ in the expression will contribute sub-dominantly. Upon integrating the loop momentum k , these terms lead to $p_i \cdot p_j = m_e^2$ or $p_i \cdot q = 0$, as $q \cdot q = 0$.
- (2) Due to the propagators, Eq. (3.13) exhibits a pole around $k^2 \sim v_{\text{SM}}^2$ if the neutral scalar masses in the visible sector are of $\mathcal{O}(v_{\text{SM}})$. Consequently, the dominant contribution to d_e is expected to occur when $k^2 \sim v_{\text{SM}}^2$.

3.4.1 The heavy dark sector limit

With the property (2), the general formula can be simplified when the unknown dark sector is significantly heavier than the electroweak scale, $M \gg v_{\text{SM}}$. By power expanding $F_{\text{DS}}^{\phi_j \eta_a}(k^2, M^2)$ in terms of $v_{\text{SM}}^2/M^2 (\sim k^2/M^2)$, we can simplify $F_{\text{DS}}^{\phi_j \eta_a}$ as

$$F_{\text{DS}}^{\phi_j \eta_a}((k+q)^2, M^2) = a_0^{\phi_j \eta_a}(M^2) + a_1^{\phi_j \eta_a}(M^2) \frac{(k+q)^2}{M^2} + \mathcal{O}\left(\frac{(k+q)^4}{M^4}\right), \tag{3.16}$$

where $a_{0,1}^{\phi_j \eta_a}(M^2)$ are independent of k , and each order is expected to be suppressed by $\mathcal{O}(v_{\text{SM}}^2/M^2)$. With this expansion, the electron EDM can be explicitly calculated for the

heavy dark sector (HDS). The leading results are (see appendix D.2 for derivation):

$$d_e^{f,W} \simeq \sum_{j=1}^{N_E} \sum_{a=2}^{N_O} \sum_{\Phi=\phi_j, \eta_a} \int_x \frac{g_{eG}^V \left(C_E^{f,W} g_{e\Phi}^P - C_O^{f,W} g_{e\Phi}^S \right)}{16\pi^2 m_{\phi_j}^2} \times \left[\frac{a_0^{\phi_j \eta_a}(M^2)}{m_{\phi_j}^2} j_3^{(1)}(r_{f,W}, r_G, r_{\eta_a}) + \frac{a_1^{\phi_j \eta_a}(M^2)}{M^2} j_3^{(2)}(r_{f,W}, r_G, r_{\eta_a}) \right], \quad (3.17)$$

where we omit terms proportional to $m_e^2/m_{\phi_j}^2 \sim m_e^2/v_{\text{SM}}^2$. The integrals of momentum k and the Feynman parameter y have been calculated explicitly. Here, r_{f,W,G,η_a} are mass squared ratios defined as

$$r_{f,W} \equiv \frac{m_{f,W}^2}{m_{\phi_j}^2 x(1-x)}, \quad r_G \equiv \frac{m_G^2}{m_{\phi_j}^2}, \quad r_{\eta_a} \equiv \frac{m_{\eta_a}^2}{m_{\phi_j}^2}. \quad (3.18)$$

The coefficients $C_E^{f,W}$ and $C_O^{f,W}$ encapsulate the information from the inner fermion and W boson loops, and they are defined as [37, 47]:

$$C_E^f = + \frac{N_C^f}{4\pi^2} g_{f\gamma}^V g_{fG}^V g_{f\Phi}^S m_f \left[x^2 + (1-x)^2 \right], \quad (3.19)$$

$$C_O^f = - \frac{N_C^f}{4\pi^2} g_{f\gamma}^V g_{fG}^V g_{f\Phi}^P m_f, \quad (3.20)$$

$$C_E^W = + \frac{e}{8\pi^2} g_{WW\Phi} g_{WWG} \left\{ \left(4 - \frac{m_G^2}{m_W^2} \right) - \frac{x(1-x)}{2} \left[6 - \frac{m_G^2}{m_W^2} + \left(1 - \frac{m_G^2}{2m_W^2} \right) \frac{m_\Phi^2}{m_W^2} \right] \right\}, \quad (3.21)$$

$$C_O^W = 0, \quad (3.22)$$

where $g_{WW\Phi} = \frac{2m_W^2}{v_{\text{SM}}} \xi_{\phi_j}^W$ (0) for CP-even (CP-odd) scalar, and $g_{WWG} = e \cos \theta_W / \sin \theta_W$ (e) for $G = Z(\gamma)$. The function $j_3^{(1,2)}(r_{f,W}, r_G, r_{\eta_a})$, arising from the integration of Feynman parameters, is defined by

$$j_3^{(n)}(r_{f,W}, r_G, r_{\eta_a}) \equiv \frac{r_{f,W}^n \ln r_{f,W}}{(r_{f,W} - 1)(r_{f,W} - r_G)(r_{f,W} - r_{\eta_a})} + \frac{r_G^n \ln r_G}{(r_G - 1)(r_G - r_{f,W})(r_G - r_{\eta_a})} + \frac{r_{\eta_a}^n \ln r_{\eta_a}}{(r_{\eta_a} - 1)(r_{\eta_a} - r_{f,W})(r_{\eta_a} - r_G)}. \quad (3.23)$$

For the case where the gauge boson is the photon, i.e., $G = \gamma$ ($m_G = 0$), the function j_3 becomes:

$$j_3^{(n)}(r_{f,W}, 0, r_{\eta_a}) = \frac{r_{f,W}^{n-1} \ln r_{f,W}}{(r_{f,W} - 1)(r_{f,W} - r_{\eta_a})} + \frac{r_{\eta_a}^{n-1} \ln r_{\eta_a}}{(r_{\eta_a} - 1)(r_{\eta_a} - r_{f,W})}. \quad (3.24)$$

H_1	H_2	S	Q_L	u_R	d_R	L_L	e_R
i^2	1	i	1	1	z_4^d	1	z_4^e

Table 4: We present an example of Z_4 charges for the scalar dark sector model. The exact values of z_4^d and z_4^e for the right-handed d quark and electron depend on the specific type of the 2HDM being considered.

4 Numerical analysis for benchmark models

In the previous section, we have derived the formula for the electron EDM in a general CP-violating dark sector. Let us now consider two specific dark sector models. The first model consists of a complex singlet scalar whose potential contains CP violation (the scalar dark sector model). The second model involves a vector-like singlet fermion with a CP-violating Yukawa coupling and a complex singlet scalar portal to the Higgs sector (the fermion dark sector model). For both models, we numerically estimate the size of the electron EDM and discuss the validity of the expression in the HDS limit.

4.1 Scalar dark sector model

We introduce a complex singlet scalar denoted as S . Its mass term and self-interactions are described by the potential V_{DS} . In addition, we allow for interactions between the scalar S and the Higgs doublets of the 2HDM through the potential V_{HO} . The expressions for V_{DS} and V_{HO} are given by

$$V_{\text{DS}} = m_S^2 |S|^2 + \frac{\lambda_S}{2} |S|^4 + [B_S S^2 + D_S S^4 + \text{h.c.}], \quad (4.1)$$

$$V_{\text{HO}} = \lambda_{1S} H_1^\dagger H_1 |S|^2 + \lambda_{2S} H_2^\dagger H_2 |S|^2 + [\lambda_{12S} H_1^\dagger H_2 S^2 + \lambda_{21S} H_2^\dagger H_1 S^2 + \text{h.c.}]. \quad (4.2)$$

In our analysis, we parameterize the complex scalar as $S = (s_1 + is_2)/\sqrt{2}$. To simplify and focus on relevant terms in V_{DS} and V_{HO} , we impose a discrete Z_4 symmetry, and its charges are summarized in Table 4. According to the charge assignment of S , B_S is a soft Z_4 breaking term.⁵

There are 6 complex parameters in the scalar potential of the model: m_{12}^2 and λ_5 in Eq. (2.1) and B_S , D_S , λ_{12S} and λ_{21S} in $V_{\text{DS}} + V_{\text{HO}}$. To explore CP violation, it is advantageous to identify rephasing-invariant phases, as studied in refs. [49, 50]. The details are discussed in appendix C.1, where we have five invariant phases. For our analysis, the relevant invariant phase in the dark sector is

$$\theta_{\text{phys}} = \arg [B_S^2 D_S^*]. \quad (4.3)$$

⁵Due to the remaining Z_2 symmetry, S may become a DM candidate.

While D_S is, in principle, a complex parameter, we can select the phase of S to render it real. Consequently, in this scenario, the physical phase θ_{phys} is dictated by the phase of B_S , resulting in tree-level CP violation in the mass mixing matrix for the S scalars. In appendix C.1, another invariant phase $\arg[B_S^2 \lambda_{12S}^* \lambda_{21S}^*]$ can also induce the same tree-level CP violation once $H_{1,2}$ acquire their VEVs. However, given our assumption of CP violation happening in the dark sector only, we set $\arg[B_S^2 \lambda_{12S}^* \lambda_{21S}^*] = 0$ to maintain simplicity in the CP violation pattern. Thus, in our analysis, we turn off all the physical phases other than Eq. (4.3).

Our assumption (i) in section 2.2 requires that the scalar field S does not acquire a nonzero VEV. Therefore, the CP-violating phase in B_S contributes to the mass matrix of the dark scalars $s_{1,2}$, resulting in CP-violating mixing. Explicitly, the mass matrix for the complex scalar S is given in the basis of (s_1, s_2) as

$$M_s^2 = \bar{m}_S^2 \mathbf{1}_{2 \times 2} + \begin{pmatrix} \text{Re}(\bar{B}_S) & -\text{Im}(\bar{B}_S) \\ -\text{Im}(\bar{B}_S) & -\text{Re}(\bar{B}_S) \end{pmatrix}, \quad (4.4)$$

with $\bar{m}_S^2 \equiv m_S^2 + \frac{1}{2} \lambda_{1S} v_1^2 + \frac{1}{2} \lambda_{2S} v_2^2$ and $\bar{B}_S \equiv 2B_S + (\lambda_{12S} + \lambda_{21S}) v_1 v_2$. Note that since the neutral scalars in the 2HDM sector and $s_{1,2}$ do not mix with each other, the SM Yukawa couplings and the W boson couplings are not modified from Eq. (2.7) with coefficients $\xi_{h,H,A}^f$ in Table 2 and Eq. (2.8). As a result, we obtain the following new mass eigenstates $\varphi_{1,2}$:

$$\varphi_1 = s_1 c_{\theta_s} + s_2 s_{\theta_s}, \quad \varphi_2 = -s_1 s_{\theta_s} + s_2 c_{\theta_s}, \quad (4.5)$$

where θ_s is a mixing angle with $m_{\varphi_1}^2 < m_{\varphi_2}^2$, and its value is determined by

$$\sin 2\theta_s = \frac{\text{Im}(\bar{B}_S)}{|\bar{B}_S|}. \quad (4.6)$$

When we assume the portal couplings λ_{12S} and λ_{21S} to be real, θ_s becomes a phase of B_S and corresponds to the physical CP-violating phase. The mass eigenvalues are given by

$$m_{\varphi_1}^2 = \bar{m}_S^2 - |\bar{B}_S|, \quad m_{\varphi_2}^2 = \bar{m}_S^2 + |\bar{B}_S|. \quad (4.7)$$

Incorporating all the mass eigenstates into the potentials, we can derive the corresponding neutral scalar cubic and quartic couplings as

$$\begin{aligned} V_{\text{scl}} = V_H + V_{H\phi} + V_{D_S} \supset & \frac{v_{\text{SM}}}{2} \left(\lambda_{hjk} h^0 \varphi_j \varphi_k + \lambda_{Hjk} H^0 \varphi_j \varphi_k + \lambda_{Ajk} A^0 \varphi_j \varphi_k \right) \\ & + \frac{1}{2} \left(\lambda_{hAjj} h^0 A^0 \varphi_j \varphi_j + \lambda_{HAjj} H^0 A^0 \varphi_j \varphi_j \right), \end{aligned} \quad (4.8)$$

λ_{h11}	$-\lambda_{1S}s_\alpha c_\beta + \lambda_{2S}c_\alpha s_\beta + (\lambda_{12S} + \lambda_{21S})c_{\alpha+\beta}c_{2\theta_s}$
λ_{h12}	$-2(\lambda_{12S} + \lambda_{21S})c_{\alpha+\beta}s_{2\theta_s}$
λ_{h22}	$-\lambda_{1S}s_\alpha c_\beta + \lambda_{2S}c_\alpha s_\beta - (\lambda_{12S} + \lambda_{21S})c_{\alpha+\beta}c_{2\theta_s}$
λ_{H11}	$\lambda_{1S}c_\alpha c_\beta + \lambda_{2S}s_\alpha s_\beta + (\lambda_{12S} + \lambda_{21S})s_{\alpha+\beta}c_{2\theta_s}$
λ_{H12}	$-2(\lambda_{12S} + \lambda_{21S})s_{\alpha+\beta}s_{2\theta_s}$
λ_{H22}	$\lambda_{1S}c_\alpha c_\beta + \lambda_{2S}s_\alpha s_\beta - (\lambda_{12S} + \lambda_{21S})s_{\alpha+\beta}c_{2\theta_s}$
λ_{A11}	$-(\lambda_{12S} - \lambda_{21S})s_{2\theta_s}$
λ_{A12}	$-2(\lambda_{12S} - \lambda_{21S})c_{2\theta_s}$
λ_{A22}	$(\lambda_{12S} - \lambda_{21S})s_{2\theta_s}$
λ_{hA11}	$(\lambda_{12S} - \lambda_{21S})s_{\alpha-\beta}s_{2\theta_s}$
λ_{hA22}	$-(\lambda_{12S} - \lambda_{21S})s_{\alpha-\beta}s_{2\theta_s}$
λ_{HA11}	$-(\lambda_{12S} - \lambda_{21S})c_{\alpha-\beta}s_{2\theta_s}$
λ_{HA22}	$(\lambda_{12S} - \lambda_{21S})c_{\alpha-\beta}s_{2\theta_s}$

Table 5: The relevant neutral scalar cubic and quartic couplings. For instance, λ_{h12} represents the trilinear coupling involving the mass eigenstate of the SM Higgs and the dark sector scalars φ_1 and φ_2 .

where $j, k = 1, 2$ and each coupling is summarized in Table 5.

With the cubic and quartic couplings determined, we can now explicitly calculate the one-loop contributions from the dark sector scalars to the two effective CP-violating mixing terms F_{DS}^{hA} and F_{DS}^{HA} , as shown in the diagrams of Fig. 3,

$$\begin{aligned}
F_{\text{DS}}^{hA}(k^2) = & -\frac{v_{\text{SM}}^2}{64\pi^2}\lambda_{12S}^-s_{2\theta_s}\left[\lambda_{12S}^+c_{\alpha+\beta}c_{2\theta_s}\left(\text{DiscB}(k^2, m_{\varphi_1}, m_{\varphi_1}) + \text{DiscB}(k^2, m_{\varphi_2}, m_{\varphi_2})\right.\right. \\
& \left.\left.-2\text{DiscB}(k^2, m_{\varphi_1}, m_{\varphi_2}) + \frac{m_{\varphi_1}^2 - m_{\varphi_2}^2}{k^2}\ln\frac{m_{\varphi_1}^2}{m_{\varphi_2}^2}\right) \right. \\
& \left. + \lambda_{hS}\left(\text{DiscB}(k^2, m_{\varphi_1}, m_{\varphi_1}) - \text{DiscB}(k^2, m_{\varphi_2}, m_{\varphi_2}) - \ln\frac{m_{\varphi_1}^2}{m_{\varphi_2}^2}\right)\right] \\
& + \frac{\lambda_{12S}^-}{32\pi^2}s_{\alpha-\beta}s_{2\theta_s}\left[\left(m_{\varphi_1}^2 - m_{\varphi_2}^2\right)\Lambda_{\text{UV}}^2 + m_{\varphi_1}^2\ln\frac{\mu^2}{m_{\varphi_1}^2} - m_{\varphi_2}^2\ln\frac{\mu^2}{m_{\varphi_2}^2}\right], \quad (4.9)
\end{aligned}$$

$$\begin{aligned}
F_{\text{DS}}^{HA}(k^2) = & -\frac{v_{\text{SM}}^2}{64\pi^2}\lambda_{12S}^-s_{2\theta_s}\left[\lambda_{12S}^+s_{\alpha+\beta}c_{2\theta_s}\left(\text{DiscB}(k^2, m_{\varphi_1}, m_{\varphi_1}) + \text{DiscB}(k^2, m_{\varphi_2}, m_{\varphi_2})\right.\right. \\
& \left.\left.-2\text{DiscB}(k^2, m_{\varphi_1}, m_{\varphi_2}) + \frac{m_{\varphi_1}^2 - m_{\varphi_2}^2}{k^2}\ln\frac{m_{\varphi_1}^2}{m_{\varphi_2}^2}\right) \right.
\end{aligned}$$

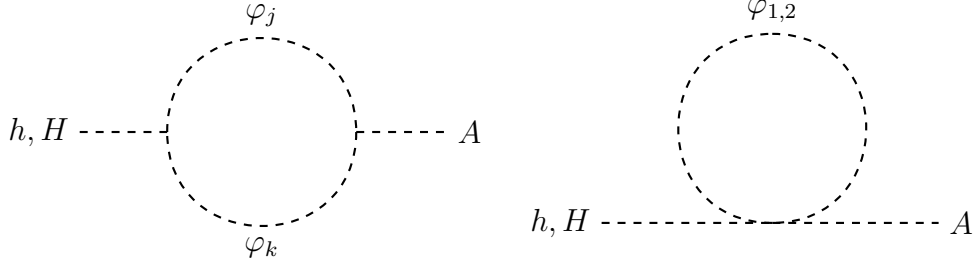


Figure 3: One-loop diagrams relevant to the effective h - A and H - A mixings induced by $\varphi_{1,2}$ in the scalar dark sector model.

$$\begin{aligned}
& + \lambda_{HS} \left(\text{DiscB}(k^2, m_{\varphi_1}, m_{\varphi_1}) - \text{DiscB}(k^2, m_{\varphi_2}, m_{\varphi_2}) - \ln \frac{m_{\varphi_1}^2}{m_{\varphi_2}^2} \right) \\
& - \frac{\lambda_{12S}^-}{32\pi^2} c_{\alpha-\beta} s_{2\theta_s} \left[(m_{\varphi_1}^2 - m_{\varphi_2}^2) \Lambda_{UV}^2 + m_{\varphi_1}^2 \ln \frac{\mu^2}{m_{\varphi_1}^2} - m_{\varphi_2}^2 \ln \frac{\mu^2}{m_{\varphi_2}^2} \right]. \quad (4.10)
\end{aligned}$$

Here, we have defined the shorthand notations $\lambda_{12S}^\pm \equiv \lambda_{12S} \pm \lambda_{21S}$, $\lambda_{hS} \equiv -\lambda_{1S} s_\alpha c_\beta + \lambda_{2S} c_\alpha s_\beta$ and $\lambda_{HS} \equiv \lambda_{1S} c_\alpha c_\beta + \lambda_{2S} s_\alpha s_\beta$. The function $\text{DiscB}(k^2, m_1, m_2)$ is defined as

$$\text{DiscB}(k^2, m_1, m_2) = \frac{\lambda^{1/2}(k^2, m_1^2, m_2^2)}{k^2} \ln \frac{m_1^2 + m_2^2 - k^2 + \lambda^{1/2}(k^2, m_1^2, m_2^2)}{2m_1 m_2}, \quad (4.11)$$

$$\lambda(k^2, m_1^2, m_2^2) = k^4 + m_1^4 + m_2^4 - 2k^2 m_1^2 - 2k^2 m_2^2 - 2m_1^2 m_2^2, \quad (4.12)$$

and Λ_{UV} and μ are a UV divergent parameter and 't Hooft mass parameter, respectively.

To obtain a finite physical prediction, we need to deal with the UV divergent part appropriately. For this purpose, let us consider the wave function renormalization for h - A and H - A self-energies [51, 52]⁶. First, we define the renormalized two-point functions $\hat{\Sigma}_{hA, HA}(k^2)$ as

$$\hat{\Sigma}_{hA}(k^2) \equiv F_{\text{DS}}^{hA}(k^2) + \frac{1}{2}(k^2 - m_h^2) \delta Z_{hA} + \frac{1}{2}(k^2 - m_A^2) \delta Z_{Ah}, \quad (4.15)$$

⁶To deal with the UV divergent in these self-energies, there is another technique for renormalization, so-called ‘‘CP-odd tadpole renormalization’’ proposed in ref. [53] (see also refs. [54, 55] for its application to the supersymmetric models). This method is basically equivalent to the wave function renormalization, since there is an explicit correspondence in contributions from CP-odd counterterm T_A and renormalization constants δZ_{hA} , δZ_{Ah} , δZ_{HA} , δZ_{AH} in Eqs. (4.15) and (4.16) as

$$\frac{T_A}{v_{\text{SM}}} s_{\alpha-\beta} \longleftrightarrow \frac{1}{2}(k^2 - m_h^2) \delta Z_{hA} + \frac{1}{2}(k^2 - m_A^2) \delta Z_{Ah}, \quad (4.13)$$

$$-\frac{T_A}{v_{\text{SM}}} c_{\alpha-\beta} \longleftrightarrow \frac{1}{2}(k^2 - m_H^2) \delta Z_{HA} + \frac{1}{2}(k^2 - m_A^2) \delta Z_{AH}, \quad (4.14)$$

where each left-hand side is obtained by the CP-odd tadpole renormalization. We found that the UV divergent parts of each contribution are totally same. Note that in this model, we have loop-induced CP-odd tadpole contributions by using λ_{A11} and λ_{A22} couplings in Table 5, which are UV divergent ones. Refs. [51, 56–60] have discussed about this divergence via Fleischer-Jegerlehner tadpole scheme [61].

$$\hat{\Sigma}_{HA}(k^2) \equiv F_{\text{DS}}^{HA}(k^2) + \frac{1}{2}(k^2 - m_H^2)\delta Z_{HA} + \frac{1}{2}(k^2 - m_A^2)\delta Z_{AH}. \quad (4.16)$$

In the on-shell subtraction scheme, we can determine $\delta Z_{hA,HA}$ and $\delta Z_{Ah,AH}$ by

$$\text{Re}\{\hat{\Sigma}_{hA}(m_h^2)\} = 0, \quad \text{Re}\{\hat{\Sigma}_{HA}(m_H^2)\} = 0, \quad \text{Re}\{\hat{\Sigma}_{hA,HA}(m_A^2)\} = 0. \quad (4.17)$$

By solving these equations, the renormalized two-point functions $\hat{\Sigma}_{hA,HA}(k^2)$ are given by

$$\hat{\Sigma}_{hA}(k^2) = F_{\text{DS}}^{hA}(k^2) + \frac{1}{m_h^2 - m_A^2} \left[(m_A^2 - k^2) \text{Re}\{F_{\text{DS}}^{hA}(m_h^2)\} + (k^2 - m_h^2) \text{Re}\{F_{\text{DS}}^{hA}(m_A^2)\} \right], \quad (4.18)$$

$$\hat{\Sigma}_{HA}(k^2) = F_{\text{DS}}^{HA}(k^2) + \frac{1}{m_H^2 - m_A^2} \left[(m_A^2 - k^2) \text{Re}\{F_{\text{DS}}^{HA}(m_H^2)\} + (k^2 - m_H^2) \text{Re}\{F_{\text{DS}}^{HA}(m_A^2)\} \right]. \quad (4.19)$$

One can easily check that the divergent parts (and also other constant terms concerning the momentum k) are canceled, and hence, $\hat{\Sigma}_{hA,HA}$ give finite results. For numerical predictions, we need to replace $F_{\text{DS}}^{hA} \rightarrow \hat{\Sigma}_{hA}$ and $F_{\text{DS}}^{HA} \rightarrow \hat{\Sigma}_{HA}$ in the expressions that we have obtained in the previous section.

In the HDS approximation, the dark sector scalar masses $m_{\varphi_1}, m_{\varphi_2}$ are much larger than the masses in the 2HDM. In this case, we can expand $\hat{\Sigma}_{hA(HA)}(k^2)$ as

$$\hat{\Sigma}_{hA(HA)}(k^2) = a_0^{hA(HA)} + a_1^{hA(HA)} \frac{k^2}{m_{\varphi_1} m_{\varphi_2}} + \mathcal{O}\left(\frac{k^4}{m_{\varphi_i}^4}\right), \quad (4.20)$$

where we choose M^2 in Eq. (3.16) to be $m_{\varphi_1} m_{\varphi_2}$. Each coefficient is given explicitly as

$$\begin{aligned} a_0^{hA} = & \frac{v_{\text{SM}}^2 \lambda_{12S}^-}{64\pi^2} s_{2\theta_s} \left[\lambda_{12S}^+ c_{\alpha+\beta} c_{2\theta_s} \left(2 + \left\{ \frac{m_{\varphi_1}^2 - m_{\varphi_2}^2}{m_h^2} + \frac{m_{\varphi_1}^2 - m_{\varphi_2}^2}{m_A^2} - \frac{m_{\varphi_1}^2 + m_{\varphi_2}^2}{m_{\varphi_1}^2 - m_{\varphi_2}^2} \right\} \ln \frac{m_{\varphi_1}^2}{m_{\varphi_2}^2} \right. \right. \\ & \left. \left. + \frac{1}{m_h^2 - m_A^2} \left[m_h^2 \mathcal{F}_1(m_A, m_{\varphi_1}, m_{\varphi_2}) - m_A^2 \mathcal{F}_1(m_h, m_{\varphi_1}, m_{\varphi_2}) \right] \right) \right. \\ & \left. + \frac{\lambda_{hS}}{m_h^2 - m_A^2} \left(m_h^2 \mathcal{F}_2(m_A, m_{\varphi_1}, m_{\varphi_2}) - m_A^2 \mathcal{F}_2(m_h, m_{\varphi_1}, m_{\varphi_2}) \right) \right], \quad (4.21) \end{aligned}$$

$$\begin{aligned} a_1^{hA} = & -\frac{v_{\text{SM}}^2 \lambda_{12S}^-}{64\pi^2} s_{2\theta_s} \left[\lambda_{12S}^+ c_{\alpha+\beta} c_{2\theta_s} \left(\frac{(m_{\varphi_1}^2 + m_{\varphi_2}^2)(m_{\varphi_1}^4 - 8m_{\varphi_1}^2 m_{\varphi_2}^2 + m_{\varphi_2}^4)}{6m_{\varphi_1} m_{\varphi_2} (m_{\varphi_1}^2 - m_{\varphi_2}^2)^2} \right. \right. \\ & \left. \left. + \left\{ \frac{(m_{\varphi_1}^2 - m_{\varphi_2}^2)m_{\varphi_1} m_{\varphi_2}}{m_h^2 m_A^2} + \frac{2m_{\varphi_1}^3 m_{\varphi_2}^3}{(m_{\varphi_1}^2 - m_{\varphi_2}^2)^3} \right\} \ln \frac{m_{\varphi_1}^2}{m_{\varphi_2}^2} \right. \right. \\ & \left. \left. - \frac{m_{\varphi_1} m_{\varphi_2}}{m_h^2 - m_A^2} \left[\mathcal{F}_1(m_h, m_{\varphi_1}, m_{\varphi_2}) - \mathcal{F}_1(m_A, m_{\varphi_1}, m_{\varphi_2}) \right] \right) \right] \end{aligned}$$

$$- \lambda_{hS} \left(\frac{m_{\varphi_1}^2 - m_{\varphi_2}^2}{6m_{\varphi_1}m_{\varphi_2}} + \frac{m_{\varphi_1}m_{\varphi_2}}{m_h^2 - m_A^2} \left[\mathcal{F}_2(m_h, m_{\varphi_1}, m_{\varphi_2}) - \mathcal{F}_2(m_A, m_{\varphi_1}, m_{\varphi_2}) \right] \right), \quad (4.22)$$

$$a_0^{HA} = \frac{v_{\text{SM}}^2 \lambda_{12S}^-}{64\pi^2} s_{2\theta_s} \left[\lambda_{12S}^+ s_{\alpha+\beta} c_{2\theta_s} \left(2 + \left\{ \frac{m_{\varphi_1}^2 - m_{\varphi_2}^2}{m_H^2} + \frac{m_{\varphi_1}^2 - m_{\varphi_2}^2}{m_A^2} - \frac{m_{\varphi_1}^2 + m_{\varphi_2}^2}{m_{\varphi_1}^2 - m_{\varphi_2}^2} \right\} \ln \frac{m_{\varphi_1}^2}{m_{\varphi_2}^2} \right. \right. \\ \left. \left. + \frac{1}{m_H^2 - m_A^2} \left[m_H^2 \mathcal{F}_1(m_A, m_{\varphi_1}, m_{\varphi_2}) - m_A^2 \mathcal{F}_1(m_H, m_{\varphi_1}, m_{\varphi_2}) \right] \right) \right. \\ \left. + \frac{\lambda_{HS}}{m_H^2 - m_A^2} \left(m_H^2 \mathcal{F}_2(m_A, m_{\varphi_1}, m_{\varphi_2}) - m_A^2 \mathcal{F}_2(m_H, m_{\varphi_1}, m_{\varphi_2}) \right) \right], \quad (4.23)$$

$$a_1^{HA} = -\frac{v_{\text{SM}}^2 \lambda_{12S}^-}{64\pi^2} s_{2\theta_s} \left[\lambda_{12S}^+ s_{\alpha+\beta} c_{2\theta_s} \left(\frac{(m_{\varphi_1}^2 + m_{\varphi_2}^2)(m_{\varphi_1}^4 - 8m_{\varphi_1}^2 m_{\varphi_2}^2 + m_{\varphi_2}^4)}{6m_{\varphi_1}m_{\varphi_2}(m_{\varphi_1}^2 - m_{\varphi_2}^2)^2} \right. \right. \\ \left. \left. + \left\{ \frac{(m_{\varphi_1}^2 - m_{\varphi_2}^2)m_{\varphi_1}m_{\varphi_2}}{m_H^2 m_A^2} + \frac{2m_{\varphi_1}^3 m_{\varphi_2}^3}{(m_{\varphi_1}^2 - m_{\varphi_2}^2)^3} \right\} \ln \frac{m_{\varphi_1}^2}{m_{\varphi_2}^2} \right. \right. \\ \left. \left. - \frac{m_{\varphi_1}m_{\varphi_2}}{m_H^2 - m_A^2} \left[\mathcal{F}_1(m_H, m_{\varphi_1}, m_{\varphi_2}) - \mathcal{F}_1(m_A, m_{\varphi_1}, m_{\varphi_2}) \right] \right) \right. \\ \left. - \lambda_{HS} \left(\frac{m_{\varphi_1}^2 - m_{\varphi_2}^2}{6m_{\varphi_1}m_{\varphi_2}} + \frac{m_{\varphi_1}m_{\varphi_2}}{m_H^2 - m_A^2} \left[\mathcal{F}_2(m_H, m_{\varphi_1}, m_{\varphi_2}) - \mathcal{F}_2(m_A, m_{\varphi_1}, m_{\varphi_2}) \right] \right) \right], \quad (4.24)$$

where we have defined the following functions:

$$\mathcal{F}_1(m, m_{\varphi_1}, m_{\varphi_2}) \equiv \text{Re}\{\text{DiscB}(m^2, m_{\varphi_1}, m_{\varphi_1})\} + \text{Re}\{\text{DiscB}(m^2, m_{\varphi_2}, m_{\varphi_2})\} \\ - 2\text{Re}\{\text{DiscB}(m^2, m_{\varphi_1}, m_{\varphi_2})\}, \quad (4.25)$$

$$\mathcal{F}_2(m, m_{\varphi_1}, m_{\varphi_2}) \equiv \text{Re}\{\text{DiscB}(m^2, m_{\varphi_1}, m_{\varphi_1})\} - \text{Re}\{\text{DiscB}(m^2, m_{\varphi_2}, m_{\varphi_2})\}. \quad (4.26)$$

Since $a_0^{hA(HA)} = \hat{\Sigma}_{\text{DS}}^{hA(HA)}(k^2 \rightarrow 0)$, they are used to calculate the coefficient of the four-fermion operator $C_{ff'}$ by inserting $a_0^{hA,HA}$ into Eq. (3.8). Therefore, we have obtained the electron EDM in the HDS approximation as well as the coefficient C_S . By applying the limit of the JILA experiment in Eq. (3.3), one can establish bounds on the parameters for the scalar dark sector model.

4.1.1 Numerical results

Let us now perform the numerical analysis for the scalar dark sector model. We choose the following values for the relevant masses and parameters:

$$m_h = 125.25 \text{ GeV}, \quad m_H = 1500 \text{ GeV}, \quad m_A = 1550 \text{ GeV}, \quad \alpha = -0.02, \quad \tan \beta = 50,$$

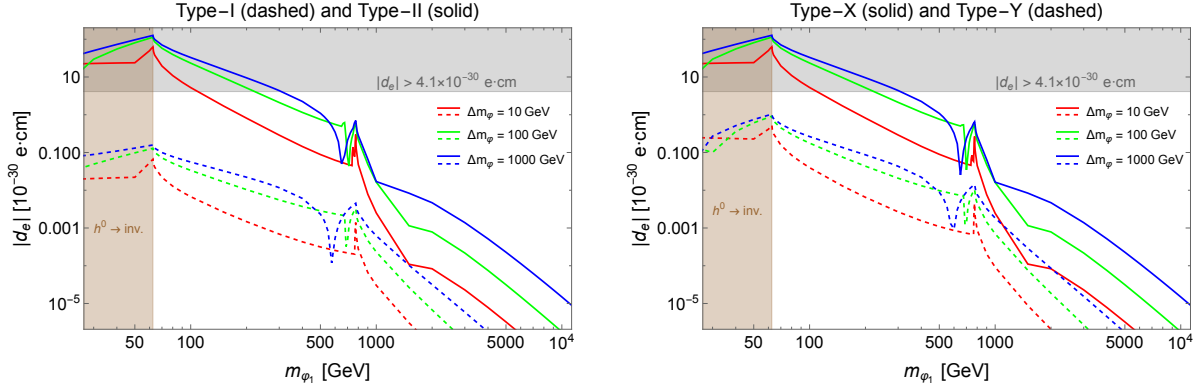


Figure 4: Numerical results of the electron EDM in the scalar dark sector model. The left panel shows the results of Type-I (dashed lines) and Type-II (solid lines) 2HDMs, while the right panel shows those of Type-X (solid lines) and Type-Y (dashed lines) 2HDMs. The color means different choices of $\Delta m_\varphi \equiv m_{\varphi_2} - m_{\varphi_1}$: $\Delta m_\varphi = 10$ GeV (red), $\Delta m_\varphi = 100$ GeV (green) and $\Delta m_\varphi = 1000$ GeV (blue). The gray shaded region is excluded by the current electron EDM bound from the JILA experiment [18], and the brown shaded region is constrained by the SM Higgs invisible decay, $h^0 \rightarrow \text{inv}$ [62].

$$\theta_s = \frac{\pi}{4}, \quad \lambda_{1S} = 1, \quad \lambda_{2S} = 2, \quad \lambda_{12S} = 2, \quad \lambda_{21S} = 0.1. \quad (4.27)$$

Note that the value of θ_s corresponds to the maximal choice for the physical CP phase. With this parameter choice, we have found that the C_S contribution is several orders of magnitude smaller than the electron EDM d_e from the BZ diagrams. Hence, we simply neglect the C_S term in the calculation.

Fig. 4 shows the size of the electron EDM d_e in terms of m_{φ_1} , with 3 choices of mass difference for $m_{\varphi_{1,2}}$: $\Delta m_\varphi \equiv m_{\varphi_2} - m_{\varphi_1} = 10$ GeV (red lines), 100 GeV (green lines) and 1000 GeV (blue lines). The left panel corresponds to the cases of Type-I (dashed lines) and Type-II (solid lines), while the right panel shows those in Type-X (solid lines) and Type-Y (dashed lines). The shaded regions are constrained by the JILA experiment for the electron EDM bound [18] (gray) and the SM Higgs invisible decay $h \rightarrow \varphi_i \varphi_j$, which leads to the exclusion of $m_{\varphi_1} < m_h/2$ (brown).

The value of the electron EDM d_e is obtained from the general expression in Eq. (3.13) by omitting $k \cdot q$ and $k \cdot p_{1,2}$ terms which give small corrections of $\mathcal{O}(m_e^2/v_{\text{SM}}^2)$. We take account of the BZ diagrams with the 3rd generation fermions and the W boson in the inner loop.

As expected from Table 2, Type-II and Type-X 2HDMs have enough $\tan \beta$ enhancement from the electron-neutral scalar couplings to reach the current upper bound on $|d_e|$, while Type-I and Type-Y 2HDMs predict several orders of magnitude smaller $|d_e|$, due to the $\tan \beta$ suppression from those couplings. We can see from Fig. 4 that Type-Y 2HDM predicts slightly larger d_e than Type-I 2HDM, due to the enhancement from the bottom quark couplings to the neutral scalars. In addition, Type-II and Type-X 2HDM cases exhibit similar predictions for $|d_e|$ because the primary contribution to $|d_e|$ arises

from the top quark and W boson loop processes which are the same for both cases. In the case of a large $\tan\beta$, the value of λ_{1S} becomes irrelevant for $|d_e|$, while the values of λ_{2S} and λ_{12S}^- are crucial to enhance $|d_e|$. The value of $|d_e|$ is also enhanced by the hierarchy between m_{φ_1} and m_{φ_2} , as observed in Fig. 4. This enhancement occurs because $\hat{\Sigma}_{hA(HA)}(k^2)$ are amplified when $m_{\varphi_2} \gg m_{\varphi_1}$, owing to the logarithmic terms involving the ratio of their masses, which can be achieved by choosing $\bar{m}_S^2 \simeq |\bar{B}_S|$ (see Eq. (4.7)). As a result, we obtain a sizable electron EDM for Type-II and Type-X 2HDMs: for instance, by choosing $(m_{\varphi_1}, m_{\varphi_2}) = (300 \text{ GeV}, 1300 \text{ GeV})$, $|d_e| \sim 4 \times 10^{-30} e \text{ cm}$ is predicted. Even for the case of $\Delta m_\varphi = 10 \text{ GeV}$, a large $|d_e|$ very close to the current upper limit can be obtained for $m_{\varphi_1} \simeq 100 \text{ GeV}$. Note that the behavior of d_e around $m_{\varphi_i} \simeq m_{h,H,A}/2$ is originated from the function $\text{Re}\{\text{DiscB}(m_{h,H,A}^2, m_{\varphi_i}, m_{\varphi_i})\}$, which has following properties:

- $\text{Re}\{\text{DiscB}(m^2, m_{\varphi_i}, m_{\varphi_i})\}$ is always negative, except for $m_{\varphi_i} = m/2$.
- For $m_{\varphi_i} = m/2$, $\text{Re}\{\text{DiscB}(m^2, m_{\varphi_i}, m_{\varphi_i})\} = 0$ and non-differentiable with respect to m or m_{φ_i} .
- $\text{Re}\{\text{DiscB}(m^2, m_{\varphi_i}, m_{\varphi_i})\} \simeq -2$ for $m \ll m_{\varphi_i}$.

For our choice of $\theta_s = \pi/4$, terms of $\text{Re}\{\text{DiscB}(m_{h,H,A}^2, m_{\varphi_1}, m_{\varphi_2})\}$ are dropped, because these are proportional to $s_{2\theta_s}c_{2\theta_s}$ (see Eqs. (4.9) and (4.10)).

4.1.2 Discussion on the HDS approximation

If $m_{\varphi_{1,2}}$ are much heavier than all neutral scalars of the 2HDM sector, the electron EDM is given by the HDS approximation shown in Eq. (3.17) along with Eqs. (4.21)-(4.24). Fig. 5 shows the numerical estimates of the electron EDM in Type-II 2HDM for $\Delta m_\varphi = 100 \text{ GeV}$, with (red dotted) and without (solid) the HDS approximation. Similar behaviors can be seen for other types and/or other Δm_φ cases. We can see from the figure that for large m_{φ_1} , both curves decrease monotonically. However, the values of $|d_e|$ are not close to each other. Moreover, even for the mass of $m_{\varphi_1} = \mathcal{O}(v_{\text{SM}})$, the HDS approximation looks good. To explain these reasons, we first parameterize d_e as

$$d_e = d_e^{\text{Org.}} + d_e^{\text{Ren.}}, \quad (4.28)$$

where $d_e^{\text{Org.}}$ and $d_e^{\text{Ren.}}$ denote the finite part of $F_{\text{DS}}^{hA,HA}$ and the finite part of terms induced by renormalization for $F_{\text{DS}}^{hA,HA}$ in Eqs. (4.18) and (4.19), whose expressions are summarized in appendix D.3. For the HDS approximation result, we add the superscript ‘‘HDS’’,

$$d_e^{\text{HDS}} = d_e^{\text{Org.,HDS}} + d_e^{\text{Ren.,HDS}}. \quad (4.29)$$

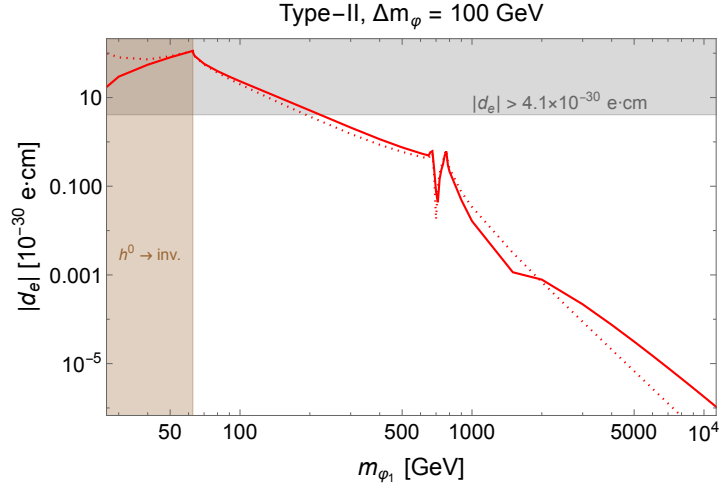


Figure 5: Numerical results of the electron EDM with (dotted line) and without (solid line) the HDS approximation in the scalar dark sector model.

Note that $d_e^{\text{Ren.}}$ and $d_e^{\text{Ren.,HDS}}$ are the same at the analytical level. Then, the difference between the results with and without the HDS approximation comes from the accuracy of calculations in $d_e^{\text{Org.}}$ and $d_e^{\text{Org.,HDS}}$.

To quantify the accuracy of the HDS approximation, we now define

$$\rho_{d_e}^{\text{Org.}} \equiv \frac{d_e^{\text{Org.,HDS}}}{d_e^{\text{Org.}}}, \quad (4.30)$$

and plot $|1 - \rho_{d_e}^{\text{Org.}}|$ in the left panel of Fig. 6. We can see that the HDS approximation agrees within 1% when $m_{\phi_1} \gtrsim 4.5 \times 10^4$ GeV. However, as parameterized in Eq. (4.28), the physical prediction is the sum of $d_e^{\text{Org.}}$ and $d_e^{\text{Ren.}}$, and therefore, a cancellation between them may affect the accuracy of the physical results. The right panel of Fig. 6 shows this feature, by defining

$$\epsilon_{d_e} \equiv \frac{d_e}{d_e^{\text{Org.}}}, \quad \epsilon_{d_e}^{\text{HDS}} \equiv \frac{d_e^{\text{HDS}}}{d_e^{\text{Org.,HDS}}}. \quad (4.31)$$

From this plot, we can understand that $|\epsilon_{d_e}|$ for the HDS approximation is much smaller than that for the result without the HDS approximation for the heavy m_{ϕ_1} region. This means that the cancellation in the HDS approximation is strong, and hence, d_e^{HDS} is predicted to be smaller than d_e , as one can see from Fig. 5. To improve the accuracy of d_e , we need to take more and more higher accuracy in the numerical integration in $d_e^{\text{Org.}}$, but it takes lots of calculation costs. We would like to emphasize that for such a heavy mass range, the prediction is far below the current upper limit, and hence, we do not need to improve the accuracy of the calculation unless the electron EDM bound is significantly improved.

Accidentally, the HDS approximation is good even for $m_{\phi_1} = \mathcal{O}(v_{\text{SM}})$. This is because around this mass range, the dominant contribution to d_e and d_e^{HDS} is coming from $d_e^{\text{Ren.}}$

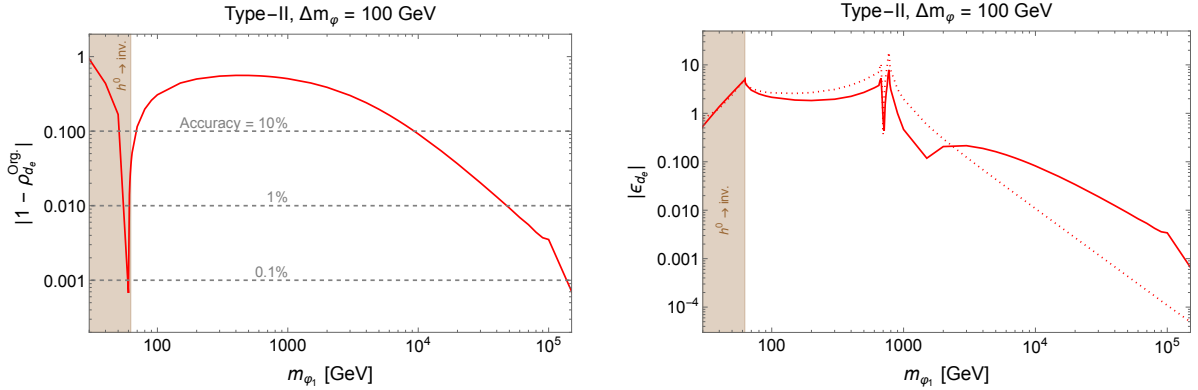


Figure 6: The left panel indicates the accuracy of the HDS approximation with $\rho_{d_e}^{\text{Org.}} \equiv d_e^{\text{Org.,HDS}}/d_e^{\text{Org.}}$, while the right panel shows the degree of cancellation in d_e (solid line) and d_e^{HDS} (dotted line) with $\epsilon_{d_e} \equiv d_e/d_e^{\text{Org.}}$ and $\epsilon_{d_e^{\text{HDS}}} \equiv d_e^{\text{HDS}}/d_e^{\text{Org.,HDS}}$. Here, we focus on the Type-II 2HDM with $\Delta m_\varphi = 100$ GeV.

which is unchanged with and without the HDS approximation. In the right panel of Fig. 6, we can see this feature directly: $|\epsilon_{d_e^{\text{HDS}}}| > 1$ means that $d_e > d_e^{\text{Org.}}$ ($d_e^{\text{HDS}} > d_e^{\text{Org.,HDS}}$), and hence, $d_e \sim d_e^{\text{Ren.}}$ ($d_e^{\text{HDS}} \sim d_e^{\text{Ren.,HDS}} = d_e^{\text{Ren.}}$).

4.2 Fermion dark sector model

Let us consider a dark sector model which contains a vector-like singlet fermion $\psi_{L,R}$ and an SM singlet complex scalar S . The dark sector Lagrangian and the scalar potential include the following terms:

$$\mathcal{L}_{\text{DS}} = -y_\psi \bar{\psi}_L \psi_R S - m_\psi \bar{\psi}_L \psi_R + \text{h.c.}, \quad (4.32)$$

$$V_{\text{scl}} \supset V_H + m_S^2 |S|^2 + \left[\mu_{1S} H_1^\dagger H_1 S + \mu_{2S} H_2^\dagger H_2 S + \mu_{12S} H_1^\dagger H_2 S + \mu_{21S} H_2^\dagger H_1 S + \text{h.c.} \right], \quad (4.33)$$

where V_H represents the scalar potential of the 2HDM sector given in Eq. (2.1).⁷ We assume a Z_2 symmetry in which H_1 and $\psi_{L,R}$ are odd. The charge assignment is summarized in Table 6. According to this Z_2 assignment, μ_{12S} and μ_{21S} terms are soft Z_2 breaking terms. It should be noted that μ_{12S} and μ_{21S} terms are necessary for the mixing among CP-odd components of $H_{1,2}$ and S (see appendix B for details). Similar to section 4.1, we parameterize S as $S = (s_1^0 + i s_2^0)/\sqrt{2}$ and assume that S does not acquire a nonzero VEV.

The model incorporates numerous complex parameters, encompassing 13 invariant phases as detailed in appendix C.2. Adhering to the presence of CP violation solely

⁷For the scalar potential, we have omitted some terms that are allowed by the charge assignment in Table 6, because these terms are irrelevant to our analysis for the electron EDM. The full scalar potential and its analysis are shown in appendix B.

H_1	H_2	S	Q_L	u_R	d_R	L_L	e_R	ψ_L	ψ_R
-	+	+	+	+	z_2^d	+	z_2^e	-	-

Table 6: The Z_2 charge assignment for the fermion dark sector model where z_2^d and z_2^e depend on the type of 2HDM.

within the dark sector, we select the following invariant phase as non-zero, contributing to the electron EDM:

$$\theta_{\text{phys}} = \arg [\mu_{1S}^* y_\psi] , \quad (4.34)$$

while assuming the other phases to be zero. Consequently, if we choose the phase of S to have real μ_{1S} , then the only CP violation happens exclusively within the Yukawa interaction of the dark sector. It is pertinent to note that a chiral phase rotation of the dark fermion $\psi_{L,R}$ has already been applied to render the mass parameter m_ψ real. Hence, we choose y_ψ to be complex and parameterize it by using two nonzero real parameters, y_ψ^R and y_ψ^I , as $y_\psi = y_\psi^R + iy_\psi^I$. Defining $\theta_\psi \equiv \arg(y_\psi)$, we also have $y_\psi^R = y_\psi \cos \theta_\psi$ and $y_\psi^I = y_\psi \sin \theta_\psi$, and θ_ψ corresponds to the physical CP phase. Consequently, we have explicit CP violation in the dark sector Yukawa couplings:

$$\mathcal{L}_{\text{CP}} = -\frac{(y_\psi^R s_1^0 - y_\psi^I s_2^0)}{\sqrt{2}} \bar{\psi} \psi - \frac{(y_\psi^I s_1^0 + y_\psi^R s_2^0)}{\sqrt{2}} \bar{\psi} i \gamma^5 \psi - m_\psi \bar{\psi} \psi . \quad (4.35)$$

The CP-even scalars (H_1^0, H_2^0, s_1^0) and the CP-odd scalars (A_1^0, A_2^0, s_2^0) are respectively expressed in terms of CP-even mass eigenstates $\phi_{1,2,3}^0$ and CP-odd mass eigenstates $\eta_{1,2,3}^0$ as

$$H_1^0 = \sum_{j=1}^3 (R_E)_{1j} \phi_j^0, \quad H_2^0 = \sum_{j=1}^3 (R_E)_{2j} \phi_j^0, \quad s_1^0 = \sum_{j=1}^3 (R_E)_{3j} \phi_j^0, \quad (4.36)$$

$$A_1^0 = \sum_{a=1}^3 (R_O)_{1a} \eta_a^0, \quad A_2^0 = \sum_{a=1}^3 (R_O)_{2a} \eta_a^0, \quad s_2^0 = \sum_{a=1}^3 (R_O)_{3a} \eta_a^0. \quad (4.37)$$

Here, we choose η_1^0 to be the neutral NG mode as mentioned in section 3.2, and hence, we can parameterize R_O by

$$R_O = \begin{pmatrix} c_\beta & -s_\beta c_{\theta_O} & s_\beta s_{\theta_O} \\ s_\beta & c_\beta c_{\theta_O} & -c_\beta s_{\theta_O} \\ 0 & s_{\theta_O} & c_{\theta_O} \end{pmatrix}, \quad (4.38)$$

where θ_O is a mixing angle between A^0 in the 2HDM sector and s_2^0 . On the other hand,

	$\xi_{\phi_j}^u$	$\xi_{\eta_a}^u$	$\xi_{\phi_j}^d$	$\xi_{\eta_a}^d$	$\xi_{\phi_j}^e$	$\xi_{\eta_a}^e$
Type-I	$(R_E)_{2j}/s_\beta$	$(R_O)_{2a} \cot \beta$	$(R_E)_{2j}/s_\beta$	$-(R_O)_{2a} \cot \beta$	$(R_E)_{2j}/s_\beta$	$-(R_O)_{2a} \cot \beta$
Type-II	$(R_E)_{2j}/s_\beta$	$(R_O)_{2a} \cot \beta$	$(R_E)_{1j}/c_\beta$	$-(R_O)_{1a} \tan \beta$	$(R_E)_{1j}/c_\beta$	$-(R_O)_{1a} \tan \beta$
Type-X	$(R_E)_{2j}/s_\beta$	$(R_O)_{2a} \cot \beta$	$(R_E)_{2j}/s_\beta$	$-(R_O)_{2a} \cot \beta$	$(R_E)_{1j}/c_\beta$	$-(R_O)_{1a} \tan \beta$
Type-Y	$(R_E)_{2j}/s_\beta$	$(R_O)_{2a} \cot \beta$	$(R_E)_{1j}/c_\beta$	$-(R_O)_{1a} \tan \beta$	$(R_E)_{2j}/s_\beta$	$-(R_O)_{2a} \cot \beta$

Table 7: The coefficients $\xi_{\phi_j}^f$ and $\xi_{\eta_a}^f$ for SM fermion Yukawa couplings in the fermion dark sector model.

R_E is parameterized by three mixing angles $\alpha, \alpha_{hS}, \alpha_{HS}$ as

$$R_E = \begin{pmatrix} c_\alpha c_{\alpha_{hS}} & -s_\alpha c_{\alpha_{HS}} - c_\alpha s_{\alpha_{hS}} s_{\alpha_{HS}} & -c_\alpha s_{\alpha_{hS}} c_{\alpha_{HS}} + s_\alpha s_{\alpha_{HS}} \\ s_\alpha c_{\alpha_{hS}} & c_\alpha c_{\alpha_{HS}} - s_\alpha s_{\alpha_{hS}} s_{\alpha_{HS}} & -s_\alpha s_{\alpha_{hS}} c_{\alpha_{HS}} - c_\alpha s_{\alpha_{HS}} \\ s_{\alpha_{hS}} & c_{\alpha_{hS}} s_{\alpha_{HS}} & c_{\alpha_{hS}} c_{\alpha_{HS}} \end{pmatrix}. \quad (4.39)$$

With these mixing angles, we can rewrite the explicit CP-violating couplings in Eq. (4.35) in terms of the scalar mass eigenstates,

$$\mathcal{L}_{\text{CP}}^{\text{Yuk}} = -\frac{1}{\sqrt{2}} \sum_{j=1}^3 \bar{\psi} (\hat{y}_{\psi,j}^R + i\hat{y}_{\psi,j}^I \gamma^5) \psi \phi_j^0 + \frac{1}{\sqrt{2}} \sum_{a=2}^3 \bar{\psi} (\tilde{y}_{\psi,a}^I - i\tilde{y}_{\psi,a}^R \gamma^5) \psi \eta_a^0, \quad (4.40)$$

where we have defined $\hat{y}_{\psi,j}^{R,I} \equiv y_{\psi}^{R,I} (R_E)_{3j}$ and $\tilde{y}_{\psi,a}^{R,I} \equiv y_{\psi}^{R,I} (R_O)_{3a}$. The SM fermion Yukawa couplings and the W boson couplings are also rewritten as

$$\mathcal{L}_{\text{Yuk}} \supset - \sum_{f=u,d,e} \frac{m_f}{v_{\text{SM}}} \left[\sum_{j=1}^3 \xi_{\phi_j}^f \bar{f} f \phi_j - \sum_{a=2}^3 \xi_{\eta_a}^f \bar{f} i \gamma^5 f \eta_a \right], \quad (4.41)$$

$$\mathcal{L} \supset \sum_{j=1}^3 \frac{2m_W^2}{v_{\text{SM}}} \xi_{\phi_j}^W W_\mu^+ W^{-\mu} \phi_j. \quad (4.42)$$

Here, $\xi_{\phi_j}^f$ and $\xi_{\eta_a}^f$ are summarized in Table 7, and $\xi_{\phi_j}^W \equiv c_\beta (R_E)_{1j} + s_\beta (R_E)_{2j}$.

With new Yukawa couplings for ψ in Eq. (4.40), the CP-violating contribution to the CP-even scalar ϕ_j and CP-odd scalar η_a mixing diagrams in Eq. (2.10) can be calculated at one-loop by running the vector-like fermion,

$$\begin{aligned} F_{\text{DS}}^{\phi_j \eta_a}(k^2) &= N_c^\psi \frac{\hat{y}_{\psi,j}^R \tilde{y}_{\psi,a}^I}{8\pi^2} m_\psi^2 \left(\Lambda_{\text{UV}}^2 - \int_0^1 dx \ln \frac{m_\psi^2 - x(1-x)k^2}{\mu^2} \right), \\ &= N_c^\psi \frac{y_{\psi}^R y_{\psi}^I}{8\pi^2} m_\psi^2 (R_E)_{3j} (R_O)_{3a} \left(\Lambda_{\text{UV}}^2 + 2 + \text{DiscB}(k^2, m_\psi, m_\psi) + \ln \frac{\mu^2}{m_\psi^2} \right), \end{aligned} \quad (4.43)$$

where Λ_{UV} denotes the UV divergent parameter, μ is the 't Hooft mass parameter and N_c^ψ represents some new color factor for the vector-like fermion ψ . In the present study, we set $N_c^\psi = 1$.

Similar to the scalar dark sector model, we need to properly handle the UV divergent part. In the current case, we consider the wave function renormalization for the $\phi_j\text{-}\eta_a$ self-energy [51, 52]. Then, the renormalized two-point function $\hat{\Sigma}_{\phi_j\eta_a}(k^2)$ is defined as

$$\hat{\Sigma}_{\phi_j\eta_a}(k^2) \equiv F_{\text{DS}}^{\phi_j\eta_a}(k^2) + \frac{1}{2}(k^2 - m_{\phi_j}^2)\delta Z_{\phi_j\eta_a} + \frac{1}{2}(k^2 - m_{\eta_a}^2)\delta Z_{\eta_a\phi_j}, \quad (4.44)$$

where no summations over j and a should be understood. In the on-shell subtraction scheme, we can determine $\delta Z_{\phi_j\eta_a}$ and $\delta Z_{\eta_a\phi_j}$ by

$$\text{Re}\{\hat{\Sigma}_{\phi_j\eta_a}(m_{\phi_j}^2)\} = 0, \quad \text{Re}\{\hat{\Sigma}_{\phi_j\eta_a}(m_{\eta_a}^2)\} = 0. \quad (4.45)$$

By solving these equations, we can obtain the renormalized two-point function $\hat{\Sigma}_{\phi_j\eta_a}(k^2)$ as

$$\begin{aligned} \hat{\Sigma}_{\phi_j\eta_a}(k^2) = \frac{y_\psi^R y_\psi^I m_\psi^2 (R_E)_{3j} (R_O)_{3a}}{8\pi^2(m_{\phi_j}^2 - m_{\eta_a}^2)} & \left[(m_{\phi_j}^2 - m_{\eta_a}^2) \text{DiscB}(k^2, m_\psi, m_\psi) \right. \\ & + (m_{\eta_a}^2 - k^2) \text{Re}\{\text{DiscB}(m_{\phi_j}^2, m_\psi, m_\psi)\} \\ & \left. + (k^2 - m_{\phi_j}^2) \text{Re}\{\text{DiscB}(m_{\eta_a}^2, m_\psi, m_\psi)\} \right], \quad (4.46) \end{aligned}$$

where the divergent part is properly canceled.

In the HDS approximation, we can further expand $\hat{\Sigma}_{\phi_j\eta_a}(k^2)$ as

$$\hat{\Sigma}_{\phi_j\eta_a}(k^2) = a_0^{\phi_j\eta_a} + a_1^{\phi_j\eta_a} \frac{k^2}{m_\psi^2} + \mathcal{O}\left(\frac{k^4}{m_\psi^4}\right). \quad (4.47)$$

Here, M^2 in Eq. (3.16) corresponds to the vector-like fermion mass m_ψ^2 , and the coefficients are

$$\begin{aligned} a_0^{\phi_j\eta_a}(m_\psi) = \frac{y_\psi^R y_\psi^I m_\psi^2 (R_E)_{3j} (R_O)_{3a}}{8\pi^2(m_{\phi_j}^2 - m_{\eta_a}^2)} & \left[-2(m_{\phi_j}^2 - m_{\eta_a}^2) - m_{\phi_j}^2 \text{Re}\{\text{DiscB}(m_{\eta_a}^2, m_\psi, m_\psi)\} \right. \\ & \left. + m_{\eta_a}^2 \text{Re}\{\text{DiscB}(m_{\phi_j}^2, m_\psi, m_\psi)\} \right], \quad (4.48) \end{aligned}$$

$$\begin{aligned} a_1^{\phi_j\eta_a}(m_\psi) = \frac{y_\psi^R y_\psi^I m_\psi^2 (R_E)_{3j} (R_O)_{3a}}{8\pi^2(m_{\phi_j}^2 - m_{\eta_a}^2)} & \left[\frac{m_{\phi_j}^2 - m_{\eta_a}^2}{6} - m_\psi^2 \text{Re}\{\text{DiscB}(m_{\phi_j}^2, m_\psi, m_\psi)\} \right. \\ & \left. + m_\psi^2 \text{Re}\{\text{DiscB}(m_{\eta_a}^2, m_\psi, m_\psi)\} \right]. \quad (4.49) \end{aligned}$$

As in the case of the scalar dark sector model, $a_0^{\phi_j\eta_a}(m_\psi)$ is used for the calculation of the four-fermion operator coefficients $C_{ff'}$.

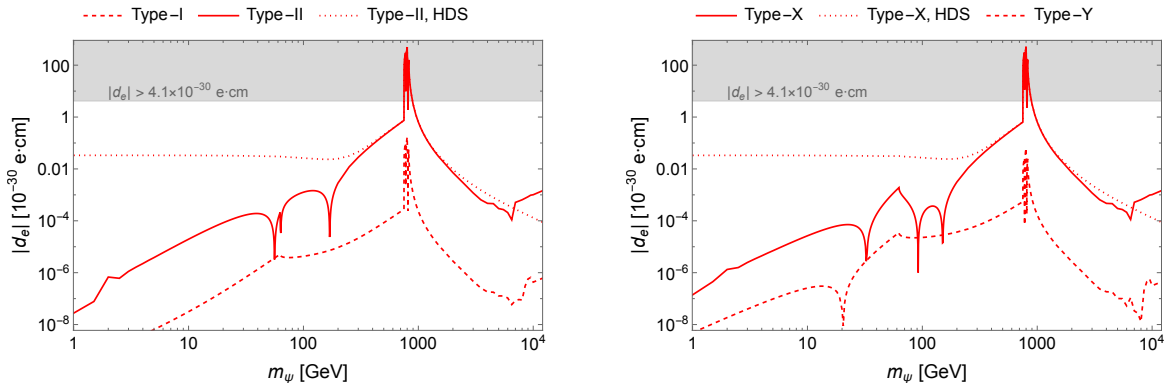


Figure 7: Numerical results of the electron EDM in the fermion dark sector model. The left panel shows the cases of Type-I (dashed line) and Type-II (solid line) 2HDMs, while the right panel shows those of Type-X (solid line) and Type-Y (dashed line) 2HDMs. The results of the HDS approximation for Type-II and Type-X 2HDMs are also shown by dotted lines in each panel. The gray-shaded region is excluded by the current electron EDM bound from the JILA experiment [18]. In this plot, we choose the parameters that satisfy the constraint of the SM Higgs invisible decay, $h^0 \rightarrow \psi\bar{\psi}$.

4.2.1 Numerical results

Similar to the scalar dark sector model, to numerically estimate the size of the electron EDM generated in the current model, we choose the following masses and parameters:

$$\begin{aligned}
 m_{\phi_1} &= 125.25 \text{ GeV}, \quad m_{\phi_2} = 1500 \text{ GeV}, \quad m_{\phi_3} = 1600 \text{ GeV}, \quad \alpha = \frac{\pi}{3}, \quad \alpha_{hS} = 0.01, \quad \alpha_{HS} = \frac{\pi}{6}, \\
 m_{\eta_2} &= 1550 \text{ GeV}, \quad m_{\eta_3} = 1650 \text{ GeV}, \quad \tan \beta = 50, \quad \theta_O = \frac{\pi}{4}, \quad y_\psi^R = y_\psi^I = \frac{1}{\sqrt{2}}. \quad (4.50)
 \end{aligned}$$

The choices of $y_\psi^{R,I}$ can be obtained by $|y_\psi| = 1$ and $\theta_\psi = \pi/4$, and the value of θ_ψ corresponds to the one which maximizes the d_e with the assumption where all parameters in V_{scl} are real. We then calculate $|d_e|$ as a function of m_ψ . The C_S contribution is found to be significantly smaller than the electron EDM contribution d_e , and hence neglected in the subsequent calculations.

The left panel of Fig. 7 presents curves for $|d_e|$ in Type-I (dashed line) and Type-II (solid line) 2HDMs, and the right panel shows those for Type-X (solid line) and Type-Y (dashed line) 2HDMs. To get those results, we have used the general expression in Eq. (3.13) by omitting $k \cdot q$ and $k \cdot p_{1,2}$ and calculated contributions from the 3rd generation fermions (t, b) and the W boson in the inner loop, as in the case of the scalar dark sector model. The gray-shaded region is excluded by the constraint from the JILA experiments [18]. We may have a constraint from the SM Higgs invisible decay, $h^0 \rightarrow \psi\bar{\psi}$, especially if the vector-like fermion is light. The branching ratio is directly proportional to $|y_\psi|^2 \sin^2 \alpha_{hS}$, making $|y_\psi|$ and α_{hS} critical parameters. Larger values of $|y_\psi|$ and/or α_{hS} tend to exclude the lower mass region $m_\psi < m_h/2$. We have checked that the parameter choice in Eq. (4.50) can avoid the constraint.

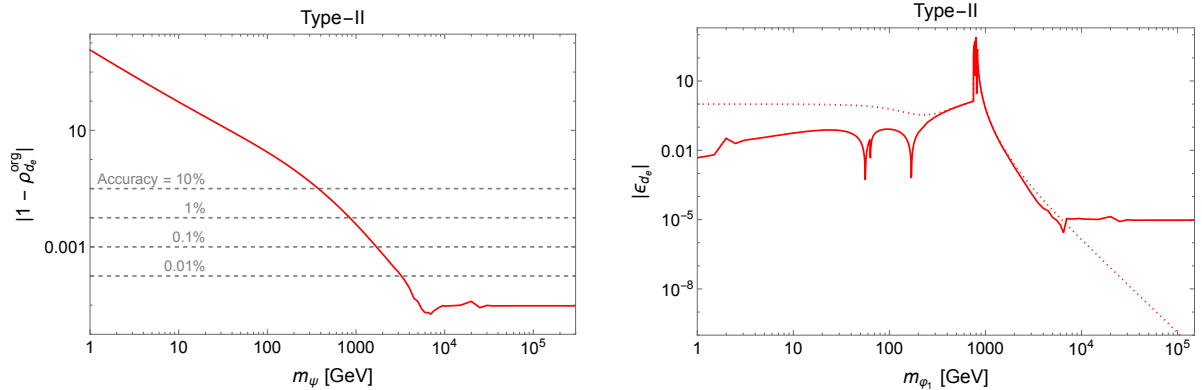


Figure 8: Plots corresponding to Fig. 6 for the fermion dark sector model.

The curves of the electron EDM $|d_e|$ in Fig. 7 show significant complexity, stemming from the m_ψ dependence of the renormalized two-point function as given in Eq. (4.46). For the region $m_\psi < 200$ GeV except for $m_\psi \simeq m_{\phi_1}/2 = m_h/2$, the sharp valleys is due to the sign flipping on d_e , while the behavior around $m_\psi \simeq m_{\phi_j}/2, m_{\eta_a}/2$ is originated from properties of functions $\text{Re}\{\text{DiscB}(m_{\phi_j}^2, m_\psi, m_\psi)\}$ and $\text{Re}\{\text{DiscB}(m_{\eta_a}^2, m_\psi, m_\psi)\}$. Notably, the region that $|d_e|$ is peaked corresponds to $m_\psi \simeq m_{\phi_j}/2$ or $m_{\eta_a}/2$, where $\hat{\Sigma}_{\phi_j\eta_a}(k^2)$ is enhanced. As in the case of the scalar dark sector model, Type-II and Type-X 2HDMs can reach the current upper limit in this mass region, while Type-I and Type-Y 2HDMs predict $|d_e|$ that is several orders of magnitude smaller than the limit. Moreover, $\hat{\Sigma}_{\phi_j\eta_a}(k^2)$ approaches to zero as m_ψ goes to zero or infinity. Such a feature is visible in Fig. 7. Note that for $m_\psi \gtrsim 7 \times 10^3$ GeV, the curves of $|d_e|$ change their behaviors, due to the low accuracy in the numerical integration, which is explained below.

4.2.2 Discussion on the HDS approximation

Remarkably, the HDS approximation results which are represented by the dotted curves for the Type-II (left panel) and Type-X (right panel) 2HDMs in Fig. 7 align well with the results without using the approximation. Note that the result for the HDS approximation can be obtained from Eq. (3.17) with Eqs. (4.48) and (4.49).

Compared with the scalar dark sector model, the HDS approximation is good, due to the simple expression for $\hat{\Sigma}_{\phi_j\eta_a}$ in Eq. (4.46) (see Eqs. (4.18) and (4.19) together with Eqs. (4.9) and (4.10) for the scalar dark sector model). Hence, we may be able to use the HDS approximation results to estimate the d_e prediction in the heavy m_ψ limit.

Fig. 8 shows $|1 - \rho_{d_e}^{\text{Org.}}|$ and $|\epsilon_{d_e}|$ which are defined in Eqs. (4.30) and (4.31), and the expressions for $d_e^{\text{Org.}}$ and $d_e^{\text{Ren.}}$ are summarized in appendix D.3. From the left panel of Fig. 8, we can see that the HDS approximation does not give the correct results for a light m_ψ , as observed from Fig. 7. On the other hand, when $m_\psi > 1000$ GeV,

the accuracy of $d_e^{\text{Org.}}$ becomes less than 1%, and hence, the HDS approximation can be used to estimate the value of the electron EDM. However, for $m_\psi \gtrsim 7 \times 10^3$ GeV, the accuracy of $d_e^{\text{Org.}}$ is saturated, and the curves with and without the HDS approximation deviate from each other (see Fig. 7). For this mass range, we need a more accurate calculation for numerical integration, which is shown in the right panel of Fig. 8. For $m_\psi \sim 7 \gtrsim 10^3$ GeV, the cancellation between $d_e^{\text{Org.}}$ and $d_e^{\text{Ren.}}$ is also saturated, at the level of $|\epsilon_{d_e}| \simeq 10^{-5}$, while that between $d_e^{\text{Org.,HDS}}$ and $d_e^{\text{Ren.,HDS}}$ decreases monotonically. Therefore, even if we obtain a good accuracy for $|1 - \rho_{d_e}^{\text{Org.}}|$, the numerical results with and without the HDS approximation deviate for the mass range of $m_\psi \gtrsim 7 \times 10^3$ GeV. As a result, for such a heavy m_ψ , the correct prediction can be obtained from the HDS approximation, although the size is far below the current upper limit on $|d_e|$.

Around $m_\psi \simeq m_{\phi_j}/2$ and $m_{\eta_a}/2$, it seems that the HDS approximation is quite good in Fig. 7. The reason is the same as that of the scalar dark sector model: in this mass region, d_e (d_e^{HDS}) is dominated by $d_e^{\text{Ren.}}$ ($d_e^{\text{Ren.,HDS}}$), as one can see from the right panel of Fig. 8.

5 Conclusion

In the present paper, we have discussed the possibility that a CP-violating dark sector coupling to the 2HDM generates a detectable electron EDM. The 2HDM was assumed to preserve the CP symmetry at the beginning, otherwise, the model is severely constrained, while the dark sector contains CP violation which is mediated to the 2HDM sector by radiative corrections. We have presented a general form of the electron EDM induced by BZ diagrams shown in Fig. 2, which can be applied to a wide range of dark sector models with CP violation.

For benchmark scenarios, we considered the scalar dark sector model and the fermion dark sector model. In the scalar dark sector model, CP violation arises in the scalar potential involving neutral Higgs and dark sector scalars. In the fermion dark sector model, a singlet complex scalar serves as a portal field, connecting a vector-like singlet fermion to the 2HDM through a complex CP-violating Yukawa coupling. For both scenarios, we carefully considered the two-point renormalized scalar self-energy functions to ensure finite results under the on-shell subtraction scheme. In each model, we found that Type-II and Type-X 2HDM cases exhibit similar predictions for $|d_e|$ and have a chance to reach the current upper limit on the electron EDM. Therefore, we can constrain the model parameter space: the mass scale of the dark sector and/or the size of effective mixing for CP-even and CP-odd scalars in the 2HDMs. The analytical expression of the electron EDM was given in the Heavy Dark Sector limit, and we have checked that it is valid to use the approximation for the estimation of the size of the electron EDM.

Since the experimental sensitivity will be improved in the future [63], the discovery of the electron EDM or its more stringent limit is expected to be obtained. In either case, our results will give important implications for physics beyond the SM with CP violation.

Acknowledgements

We would like to thank Michael Ramsey-Musolf for very helpful discussions. YN is supported by Natural Science Foundation of China under grant No. 12150610465. JL is supported by Natural Science Foundation of China under grant No. 12075005 and 12235001.

A The 2HDM

Here, we summarize mass eigenvalues and eigenstates of the 2HDM. The Higgs potential in Eq. (2.1) leads to 2×2 mass matrices for CP-even and CP-odd neutral scalars as

$$M_{\text{even}}^2 = \begin{pmatrix} m_{12}^2 \tan \beta + \lambda_1 v_1^2 & -m_{12}^2 + \lambda_{345} v_1 v_2 \\ -m_{12}^2 + \lambda_{345} v_1 v_2 & m_{12}^2 \cot \beta + \lambda_2 v_2^2 \end{pmatrix}, \quad (\text{A.1})$$

$$M_{\text{odd}}^2 = \begin{pmatrix} m_{12}^2 \tan \beta - \lambda_5 v_2^2 & -m_{12}^2 + \lambda_5 v_1 v_2 \\ -m_{12}^2 + \lambda_5 v_1 v_2 & m_{12}^2 \cot \beta - \lambda_5 v_1^2 \end{pmatrix}, \quad (\text{A.2})$$

in basis of (H_1^0, H_2^0) and (A_1^0, A_2^0) , respectively. For charged scalars, we find

$$M_{\pm}^2 = \begin{pmatrix} m_{12}^2 \tan \beta - \frac{\lambda_4 + \lambda_5}{2} v_2^2 & -m_{12}^2 + \frac{\lambda_4 + \lambda_5}{2} v_1 v_2 \\ -m_{12}^2 + \frac{\lambda_4 + \lambda_5}{2} v_1 v_2 & m_{12}^2 \cot \beta - \frac{\lambda_4 + \lambda_5}{2} v_1^2 \end{pmatrix}, \quad (\text{A.3})$$

in basis of (H_1^+, H_2^+) . Here, m_{12}^2 and λ_5 are considered as real parameters, and we define $\lambda_{345} \equiv \lambda_3 + \lambda_4 + \lambda_5$. The minimization conditions for the Higgs potential impose relations among model parameters,

$$m_1^2 = m_{12}^2 \tan \beta - \frac{1}{2} (\lambda_1 v_1^2 + \lambda_{345} v_2^2), \quad (\text{A.4})$$

$$m_2^2 = m_{12}^2 \cot \beta - \frac{1}{2} (\lambda_2 v_2^2 + \lambda_{345} v_1^2). \quad (\text{A.5})$$

The above mass matrices are diagonalized by orthogonal matrices, and each mass eigenvalue can be obtained as

$$m_h^2 = \frac{v_{\text{SM}}^2}{2} \left[(\lambda_1 c_\beta^2 + \lambda_2 s_\beta^2 + \lambda_\beta) - \sqrt{(\lambda_1 c_\beta^2 - \lambda_2 s_\beta^2 - \lambda_\beta c_{2\beta})^2 + (\lambda_{345} - \lambda_\beta)^2 s_{2\beta}^2} \right], \quad (\text{A.6})$$

$$m_H^2 = \frac{v_{\text{SM}}^2}{2} \left[(\lambda_1 c_\beta^2 + \lambda_2 s_\beta^2 + \lambda_\beta) + \sqrt{(\lambda_1 c_\beta^2 - \lambda_2 s_\beta^2 - \lambda_\beta c_{2\beta})^2 + (\lambda_{345} - \lambda_\beta)^2 s_{2\beta}^2} \right], \quad (\text{A.7})$$

$$m_A^2 = (\lambda_\beta - \lambda_5) v_{\text{SM}}^2, \quad (\text{A.8})$$

$$m_{H^\pm}^2 = \left(\lambda_\beta - \frac{1}{2} \lambda_4 - \frac{1}{2} \lambda_5 \right) v_{\text{SM}}^2 = m_A^2 - \frac{1}{2} (\lambda_4 - \lambda_5) v_{\text{SM}}^2, \quad (\text{A.9})$$

where m_h , m_H and m_A are the masses of the SM-like Higgs, heavy CP-even and CP-odd scalars, respectively, and m_{H^\pm} is the physical charged scalar mass. Here, we have defined

$$\lambda_\beta \equiv \frac{m_{12}^2}{v_1 v_2} = \frac{1}{s_\beta c_\beta} \frac{m_{12}^2}{v_{\text{SM}}^2}. \quad (\text{A.10})$$

Note that each of M_\pm^2 and M_{odd}^2 has one zero eigenvalue, which corresponds to NG modes, G^\pm and G^0 . The mass matrix for CP-even neutral scalars M_{even}^2 is diagonalized by one mixing angle α ,

$$\sin 2\alpha = \frac{(\lambda_{345} - \lambda_\beta) s_{2\beta}}{\sqrt{(\lambda_1 c_\beta^2 - \lambda_2 s_\beta^2 - \lambda_\beta c_{2\beta})^2 + (\lambda_{345} - \lambda_\beta)^2 s_{2\beta}^2}}, \quad (\text{A.11})$$

while M_\pm^2 and M_{odd}^2 are diagonalized by using $\tan \beta$ defined in Eq. (2.3). The mass eigenstates are obtained as in Eqs. (2.4) and (2.5), and for charged scalars,

$$H_1^\pm = G^\pm c_\beta - H^\pm s_\beta, \quad H_2^\pm = G^\pm s_\beta + H^\pm c_\beta, \quad (\text{A.12})$$

where H^\pm is a physical charged scalar.

B Potential analysis for the fermion dark sector model

The scalar potential of the fermion dark sector model allowed by the Z_2 charge assignments in Table 6 is given by

$$V_{\text{scl}} = V_H + V_S + V_{HS}, \quad (\text{B.1})$$

$$V_S = m_S^2 |S|^2 + \frac{\lambda_S}{2} |S|^4 + \left[\mu_2^2 S^2 + \mu_3 S |S|^2 + \mu_3' S^3 + \lambda_S' S^2 |S|^2 + \lambda_S'' S^4 + \text{h.c.} \right], \quad (\text{B.2})$$

$$V_{HS} = \left[\mu_{1S} H_1^\dagger H_1 S + \mu_{2S} H_2^\dagger H_2 S + \mu_{12S} H_1^\dagger H_2 S + \mu_{21S} H_2^\dagger H_1 S + \text{h.c.} \right] \\ + \lambda_{1S} H_1^\dagger H_1 |S|^2 + \lambda_{2S} H_2^\dagger H_2 |S|^2 + \left[\lambda_{1S}' H_1^\dagger H_1 S^2 + \lambda_{2S}' H_2^\dagger H_2 S^2 + \text{h.c.} \right]. \quad (\text{B.3})$$

We assume that all the parameters in V_{scl} are real, and S does not acquire a nonzero VEV. In the potential V_S , we can introduce a tadpole term $T_S S + \text{h.c.}$ since S is a singlet under the considered symmetries. Nevertheless, this term is removable through a shift

in S by appropriately redefining all the relevant couplings. The potential leads to the following minimization condition:

$$\mu_{1S}v_1^2 + \mu_{2S}v_2^2 + (\mu_{12S} + \mu_{21S})v_1v_2 = 0, \quad (\text{B.4})$$

with others shown in Eqs. (A.4) and (A.5). After applying all the minimization conditions, we find mass matrices for CP-even and CP-odd neutral scalars as

$$M_{\text{even}}^2 = \begin{pmatrix} \lambda_\beta v_2^2 + \lambda_1 v_1^2 & (-\lambda_\beta + \lambda_{345})v_1v_2 & \hat{m}_{1S}^2 \\ (-\lambda_\beta + \lambda_{345})v_1v_2 & \lambda_\beta v_1^2 + \lambda_2 v_2^2 & \hat{m}_{2S}^2 \\ \hat{m}_{1S}^2 & \hat{m}_{2S}^2 & m_{S,+}^2 \end{pmatrix}, \quad (\text{B.5})$$

$$M_{\text{odd}}^2 = \begin{pmatrix} (\lambda_\beta - \lambda_5)v_2^2 & (-\lambda_\beta + \lambda_5)v_1v_2 & \tilde{m}_{1S}^2 \\ (-\lambda_\beta + \lambda_5)v_1v_2 & (\lambda_\beta - \lambda_5)v_1^2 & \tilde{m}_{2S}^2 \\ \tilde{m}_{1S}^2 & \tilde{m}_{2S}^2 & m_{S,-}^2 \end{pmatrix}, \quad (\text{B.6})$$

where we define

$$\hat{m}_{1S}^2 \equiv -\frac{\sqrt{2}v_2^2}{v_1}\mu_{2S} - \frac{\mu_{12S} + \mu_{21S}}{\sqrt{2}}v_2, \quad \hat{m}_{2S}^2 \equiv \sqrt{2}\mu_{2S}v_2 + \frac{\mu_{12S} + \mu_{21S}}{\sqrt{2}}v_1, \quad (\text{B.7})$$

$$\tilde{m}_{1S}^2 \equiv \frac{\mu_{12S} - \mu_{21S}}{\sqrt{2}}v_2, \quad \tilde{m}_{2S}^2 \equiv -\frac{\mu_{12S} - \mu_{21S}}{\sqrt{2}}v_1, \quad (\text{B.8})$$

$$m_{S,\pm}^2 \equiv m_S^2 + \frac{\lambda_{1S}}{2}v_1^2 + \frac{\lambda_{2S}}{2}v_2^2 \pm (\lambda'_{1S}v_1^2 + \lambda'_{2S}v_2^2 + 2\mu_2^2), \quad (\text{B.9})$$

and λ_β is defined in Eq. (A.10). Note that terms in the first line of Eq. (B.3) are essential for mixings between neutral scalars in the 2HDM and S . In particular, if we do not introduce soft Z_2 breaking terms μ_{12S} and μ_{21S} , $\tilde{m}_{1S}^2 = 0$ and $\tilde{m}_{2S}^2 = 0$, which results in no mixing between CP-odd components of the 2HDM and S . Since S is the neutral scalar, the charged scalar mass is the same as that of the 2HDM. See appendix A.

Upon careful examination, it's apparent that the determinant of M_{odd}^2 is zero. Consequently, one of the eigenvalues derived from the matrix corresponds to the neutral NG boson field. By defining one mixing matrix for M_{odd}^2 as

$$R_{O,1} = \begin{pmatrix} c_\beta & -s_\beta & 0 \\ s_\beta & c_\beta & 0 \\ 0 & 0 & 1 \end{pmatrix}, \quad (\text{B.10})$$

we obtain

$$R_{O,1}^T M_{\text{odd}}^2 R_{O,1} = \begin{pmatrix} 0 & 0 & 0 \\ 0 & (\lambda_\beta - \lambda_5)v_{\text{SM}}^2 & -\tilde{m}_{1S}^2 s_\beta + \tilde{m}_{2S}^2 c_\beta \\ 0 & -\tilde{m}_{1S}^2 s_\beta + \tilde{m}_{2S}^2 c_\beta & m_{S,-}^2 \end{pmatrix}. \quad (\text{B.11})$$

The remaining part is diagonalized by another mixing matrix,

$$R_{O,2} = \begin{pmatrix} 1 & 0 & 0 \\ 0 & c_{\theta_O} & -s_{\theta_O} \\ 0 & s_{\theta_O} & c_{\theta_O} \end{pmatrix}, \quad (\text{B.12})$$

with the mixing angle,

$$\sin 2\theta_O = \frac{2}{\Delta m_\eta^2} (\tilde{m}_{1S}^2 s_\beta - \tilde{m}_{2S}^2 c_\beta). \quad (\text{B.13})$$

Here, Δm_η^2 is the mass-squared difference of two physical CP-odd scalars,

$$\Delta m_\eta^2 = m_{\eta_3}^2 - m_{\eta_2}^2 \quad (\text{B.14})$$

$$= \sqrt{\{(\lambda_\beta - \lambda_5) v_{\text{SM}}^2 - m_{S,-}^2\}^2 + 4(-\tilde{m}_{1S}^2 s_\beta + \tilde{m}_{2S}^2 c_\beta)^2}. \quad (\text{B.15})$$

Then, each mass eigenstate can be obtained as

$$\text{diag}(0, m_{\eta_2}^2, m_{\eta_3}^2) = R_{O,2}^T R_{O,1}^T M_{\text{odd}}^2 R_{O,1} R_{O,2} = R_O^T M_{\text{odd}}^2 R_O, \quad (\text{B.16})$$

$$m_{\eta_2}^2 = \frac{1}{2} [(\lambda_\beta - \lambda_5) v_{\text{SM}}^2 + m_{S,-}^2 - \Delta m_\eta^2], \quad (\text{B.17})$$

$$m_{\eta_3}^2 = \frac{1}{2} [(\lambda_\beta - \lambda_5) v_{\text{SM}}^2 + m_{S,-}^2 + \Delta m_\eta^2], \quad (\text{B.18})$$

where R_O is in Eq. (4.38).

In contrast to the CP-odd sector, the CP-even sector requires three mixing angles for diagonalization of M_{even}^2 , as shown in Eq. (4.39). The mixing matrix R_E is obtained as

$$R_E = R_{E,1} R_{E,2} R_{E,3}, \quad (\text{B.19})$$

$$R_{E,1} = \begin{pmatrix} c_\alpha & -s_\alpha & 0 \\ s_\alpha & c_\alpha & 0 \\ 0 & 0 & 1 \end{pmatrix}, \quad R_{E,2} = \begin{pmatrix} c_{\alpha_{hS}} & 0 & -s_{\alpha_{hS}} \\ 0 & 1 & 0 \\ s_{\alpha_{hS}} & 0 & c_{\alpha_{hS}} \end{pmatrix}, \quad R_{E,3} = \begin{pmatrix} 1 & 0 & 0 \\ 0 & c_{\alpha_{HS}} & -s_{\alpha_{HS}} \\ 0 & s_{\alpha_{HS}} & c_{\alpha_{HS}} \end{pmatrix}. \quad (\text{B.20})$$

C Rephasing-invariant CP-violating phases

We here summarize rephasing-invariant CP-violating (CPV) phases for the scalar dark sector model and the fermion dark sector model we focused on in the present paper. Detailed studies have been done in refs. [49, 50].

C.1 CPV phases in the scalar dark sector model

In the scalar potential, we have six complex parameters: $m_{12}^2, \lambda_5, B_S, D_S, \lambda_{12S}, \lambda_{21S}$, and one of VEVs of $H_{1,2}$ is generally complex, e.g., $v_1 = v_1^*$ and $v_2 = |v_2|e^{i\xi}$. Then, by considering rephases for all complex scalars as

$$H_1 \rightarrow e^{i\theta_1} H_1, \quad H_2 \rightarrow e^{i\theta_2} H_2, \quad S \rightarrow e^{i\theta_S} S, \quad (\text{C.1})$$

phases of $\theta_2 - \theta_1$ and θ_S can be absorbed by redefining all complex parameters and VEVs as

$$m_{12}^2 \rightarrow m_{12}^2 e^{i(\theta_1 - \theta_2)}, \quad \lambda_5 \rightarrow \lambda_5 e^{2i(\theta_1 - \theta_2)}, \quad v_1 v_2^* \rightarrow v_1 v_2^* e^{i(\theta_1 - \theta_2)}, \quad (\text{C.2})$$

$$B_S \rightarrow B_S e^{-2i\theta_S}, \quad D_S \rightarrow D_S e^{-4i\theta_S}, \quad (\text{C.3})$$

$$\lambda_{12S} \rightarrow \lambda_{12S} e^{i(\theta_1 - \theta_2 - 2\theta_S)}, \quad \lambda_{21S} \rightarrow \lambda_{21S} e^{i(\theta_2 - \theta_1 - 2\theta_S)}. \quad (\text{C.4})$$

As a result, the scalar potential in Eqs. (2.1), (4.1) and (4.2) is invariant under rephasing of Eq. (C.1). Then, according to the discussion in refs. [49, 50], we have the following five rephasing-invariant CPV phases:

$$\delta_{\lambda_5} = \arg [\lambda_5^* (v_1 v_2^*)^2], \quad \delta_{m_{12}^2} = \arg [(m_{12}^2)^* v_1 v_2^*], \quad \delta_S = \arg [B_S^2 D_S^*], \quad (\text{C.5})$$

$$\delta_{\lambda_{12S}} = \arg [\lambda_{12S}^* \lambda_{21S} (v_1 v_2^*)^2], \quad \delta_{\lambda_{21S}} = \arg [B_S^2 \lambda_{12S}^* \lambda_{21S}^*]. \quad (\text{C.6})$$

Note that by selecting a CP-conserving scenario within the 2HDM sector, where $m_{12}^2 = 0$, the minimization of the scalar potential implies that $\text{Im}\lambda_5 = 0$. In the case where the CPV phase only shows up in the dark sector, one could opt to assign real values to λ_{12S} and λ_{21S} , resulting in no invariant phases within the portal sector. Consequently, the sole source of CP violation would be δ_S , with D_S assumed to be real and only B_S is complex. This configuration leads to the remaining physical CP phase being expressed as Eq. (4.3).

C.2 CPV phases in the fermion dark sector model

In the relevant Lagrangian of the fermion dark sector model, we have 15 complex parameters: $y_\psi, m_\psi, m_{12}^2, \lambda_5, \mu_2^2, \mu_3, \mu_3', \mu_{1S}, \mu_{2S}, \mu_{12S}, \mu_{21S}, \lambda_S', \lambda_S'', \lambda_{1S}', \lambda_{2S}'$. Among them, m_ψ can be taken to be real by using the chiral phase rotation of $\psi_{L,R}$, as mentioned in the main text. As in the case of the scalar dark sector model, rephases for all complex scalars in Eq. (C.1) can be absorbed by redefining complex parameters as

$$y_\psi \rightarrow y_\psi e^{-i\theta_S}, \quad m_{12}^2 \rightarrow m_{12}^2 e^{i(\theta_1 - \theta_2)}, \quad \lambda_5 \rightarrow \lambda_5 e^{2i(\theta_1 - \theta_2)}, \quad v_1 v_2^* \rightarrow v_1 v_2^* e^{i(\theta_1 - \theta_2)}, \quad (\text{C.7})$$

$$\mu_2^2 \rightarrow \mu_2^2 e^{-2i\theta_S}, \quad \mu_3 \rightarrow \mu_3 e^{-i\theta_S}, \quad \mu_3' \rightarrow \mu_3' e^{-3i\theta_S}, \quad (\text{C.8})$$

$$\mu_{1S} \rightarrow \mu_{1S} e^{-i\theta_S}, \quad \mu_{2S} \rightarrow \mu_{2S} e^{-i\theta_S}, \quad (\text{C.9})$$

$$\mu_{12S} \rightarrow \mu_{12S} e^{i(\theta_1 - \theta_2 - \theta_S)}, \quad \mu_{21S} \rightarrow \mu_{21S} e^{i(\theta_2 - \theta_1 - \theta_S)}, \quad (\text{C.10})$$

$$\lambda'_S \rightarrow \lambda'_S e^{-2i\theta_S}, \quad \lambda''_S \rightarrow \lambda''_S e^{-4i\theta_S}, \quad \lambda'_{1S} \rightarrow \lambda'_{1S} e^{-2i\theta_S}, \quad \lambda'_{2S} \rightarrow \lambda'_{2S} e^{-2i\theta_S}. \quad (\text{C.11})$$

Then, we find 13 combinations for rephasing-invariant CPV phases as

$$\delta_{\lambda_5} = \arg [\lambda_5^* (v_1 v_2^*)^2], \quad \delta_{m_{12}^2} = \arg [(m_{12}^2)^* v_1 v_2^*] \quad (\text{C.12})$$

$$\delta_{\mu_2^2} = \arg [(\mu_2^2)^* y_\psi^2], \quad \delta_{\mu_3} = \arg [\mu_3^* y_\psi], \quad \delta_{\mu_3'} = \arg [(\mu_3')^* y_\psi^3], \quad (\text{C.13})$$

$$\delta_{\lambda'_S} = \arg [(\lambda'_S)^* y_\psi^2], \quad \delta_{\lambda''_S} = \arg [(\lambda''_S)^* y_\psi^4], \quad (\text{C.14})$$

$$\delta_{\mu_{1S}} = \arg [\mu_{1S}^* y_\psi], \quad \delta_{\mu_{2S}} = \arg [\mu_{2S}^* y_\psi], \quad \delta_{\mu_{12S}^* \mu_{21S}^*} = \arg [\mu_{12S}^* \mu_{21S}^* y_\psi^2], \quad (\text{C.15})$$

$$\delta_{\mu_{12S}^* \mu_{21S}} = \arg [\mu_{12S}^* \mu_{21S} (v_1 v_2^*)^2], \quad \delta_{\lambda'_{1S}} = \arg [(\lambda'_{1S})^* y_\psi^2], \quad \delta_{\lambda'_{2S}} = \arg [(\lambda'_{2S})^* y_\psi^2]. \quad (\text{C.16})$$

Again, if $m_{12}^2 = 0$, the minimization condition implies $\text{Im}\lambda_5 = 0$ which means $\delta_{\lambda_5} = 0$. However, we still have lots of CPV phases in addition to $\theta_{\text{phys}} = \delta_{\mu_{1S}}$.

D Details of calculations

In this appendix, we show the details of the calculations of the BZ diagrams.

D.1 General dark sector

Using couplings in Eq. (3.11), the left diagrams in Fig. 2 have contributions as

$$\begin{aligned} & \int \frac{d^4 k}{(2\pi)^4} i\Gamma_{f,W}^{\mu\nu} \bar{u}(p_2) \{i(g_{eG}^V \gamma^\alpha + g_{eG}^A \gamma^\alpha \gamma^5)\} \frac{i(\not{p}_2 - \not{k} + m_e)}{(p_2 - k)^2 - m_e^2} \{i(g_{e\Phi}^S + ig_{e\Phi}^P \gamma^5)\} u(p_1) \\ & \quad \times \frac{-ig_{\nu\alpha}}{k^2 - m_G^2} \frac{i}{(-k - q)^2 - m_{\eta_a}^2} \left(iF_{\text{DS}}^{\phi_j \eta_a}((-k - q)^2, M^2) \right) \frac{i}{(-k - q)^2 - m_{\phi_j}^2}, \end{aligned} \quad (\text{D.1})$$

where effective vertices of photon-gauge boson (γ/Z)-scalar $\Gamma_{f,W}^{\mu\nu}$ have information about the inner loop with fermion and W boson, respectively, G represents the photon or Z boson, and Φ is ϕ_j or η_a . Note that we should sum up all contributions for the final result. For diagrams in Fig. 2, $\Gamma_{f,W}^{\mu\nu}$ can be parameterized by

$$i\Gamma_{f,W}^{\mu\nu} = i \int_0^1 dx \frac{1}{x(1-x)} \int_0^{1-x} dy \frac{C_E^{f,W} (k^\mu q^\nu - k \cdot q g^{\mu\nu}) + C_O^{f,W} \epsilon^{\mu\nu\rho\sigma} q_\rho k_\sigma}{k^2 - \Delta_{f,W}}. \quad (\text{D.2})$$

Here, $C_E^{f,W}$ and $C_O^{f,W}$ are obtained from the inner loop calculation as [37, 47]

$$C_E^f = + \frac{N_C^f}{2\pi^2} g_{f\gamma}^V g_{fG}^V g_{f\Phi}^S m_f (1 - 4xy), \quad (\text{D.3})$$

$$C_O^f = -\frac{N_C^f}{2\pi^2} g_{f\gamma}^V g_{fG}^V g_{f\Phi}^P m_f, \quad (\text{D.4})$$

$$C_E^W = +\frac{e}{4\pi^2} g_{WW\Phi} g_{WWG} \left\{ \left(4 - \frac{m_G^2}{m_W^2} \right) - \left[6 - \frac{m_G^2}{m_W^2} + \left(1 - \frac{m_G^2}{2m_W^2} \right) \frac{m_\Phi^2}{m_W^2} \right] xy \right\}, \quad (\text{D.5})$$

$$C_O^W = 0, \quad (\text{D.6})$$

and $\Delta^{f,W}$ is defined in Eq. (3.14). Similarly, the right diagrams in Fig. 2 are

$$\begin{aligned} & \int \frac{d^4k}{(2\pi)^4} i\Gamma_{f,W}^{\mu\nu} \bar{u}(p_2) \{i(g_{e\Phi}^S + ig_{e\Phi}^P \gamma^5)\} \frac{i(\not{p}_1 + \not{k} + m_e)}{(p_1 + k)^2 - m_e^2} \{i(g_{eG}^V \gamma^\alpha + g_{eG}^A \gamma^\alpha \gamma^5)\} u(p_1) \\ & \times \frac{-ig_{\nu\alpha}}{k^2 - m_G^2} \frac{i}{(-k - q)^2 - m_{\eta_a}^2} \left(iF_{\text{DS}}^{\phi_j \eta_a}((-k - q)^2, M^2) \right) \frac{i}{(-k - q)^2 - m_{\phi_j}^2}. \end{aligned} \quad (\text{D.7})$$

Since $\Gamma_{f,W}^{\mu\nu}$ has one loop momentum k in its numerator (see Eq. (D.2)), the contributions to the electron EDM can be parameterized as

$$\text{Eq. (D.1): } \int_x \int_y \int_k \frac{A_{\alpha\beta}^{L,\Phi(f,W)} k^\alpha k^\beta + B_\alpha^{L,\Phi(f,W)} k^\alpha}{(k^2 - \Delta_{f,W}) \cdots (k^2 - 2k \cdot p_2)} F_{\text{DS}}^{\phi_j \eta_a}((k + q)^2, M^2) \sigma^{\mu\nu} \gamma^5 q_\nu, \quad (\text{D.8})$$

$$\text{Eq. (D.7): } \int_x \int_y \int_k \frac{A_{\alpha\beta}^{R,\Phi(f,W)} k^\alpha k^\beta + B_\alpha^{R,\Phi(f,W)} k^\alpha}{(k^2 - \Delta_{f,W}) \cdots (k^2 + 2k \cdot p_1)} F_{\text{DS}}^{\phi_j \eta_a}((k + q)^2, M^2) \sigma^{\mu\nu} \gamma^5 q_\nu, \quad (\text{D.9})$$

where we omit some propagators for simplicity, and $\epsilon^{\mu\nu\alpha\beta} \gamma_\alpha \gamma_\beta = -i[\gamma^\mu, \gamma^\nu] \gamma^5 = -2\sigma^{\mu\nu} \gamma^5$ is used. $A_{\alpha\beta}^{L,\Phi(f,W)}$, $A_{\alpha\beta}^{R,\Phi(f,W)}$, $B_\alpha^{L,\Phi(f,W)}$ and $B_\alpha^{R,\Phi(f,W)}$ are independent of the loop momentum k , but depend on $p_{1,2}$ and q as well as x and y through $C_{E,O}^{f,W}$. These expressions are generally obtained as

$$\begin{aligned} A_{\alpha\beta}^{L,\Phi(f,W)} &= -\frac{2}{(4m_e^2 - q^2) q^2} \left[g_{eG}^V \left(C_E^{f,W} g_{e\Phi}^P + C_O^{f,W} g_{e\Phi}^S \right) + ig_{eG}^A \left(C_E^{f,W} g_{e\Phi}^S - C_O^{f,W} g_{e\Phi}^P \right) \right] \\ & \times \left\{ 2m_e^2 (p_{1\alpha} p_{1\beta} + p_{2\alpha} p_{2\beta}) - (2m_e^2 - q^2) (p_{1\alpha} p_{2\beta} + p_{1\beta} p_{2\alpha}) \right\} \\ & + C_O^{f,W} \left(g_{eG}^V g_{e\Phi}^S - ig_{eG}^A g_{e\Phi}^P \right) g_{\alpha\beta}, \end{aligned} \quad (\text{D.10})$$

$$\begin{aligned} A_{\alpha\beta}^{R,\Phi(f,W)} &= -\frac{2}{(4m_e^2 - q^2) q^2} \left[g_{eG}^V \left(C_E^{f,W} g_{e\Phi}^P + C_O^{f,W} g_{e\Phi}^S \right) - ig_{eG}^A \left(C_E^{f,W} g_{e\Phi}^S - C_O^{f,W} g_{e\Phi}^P \right) \right] \\ & \times \left\{ 2m_e^2 (p_{1\alpha} p_{1\beta} + p_{2\alpha} p_{2\beta}) - (2m_e^2 - q^2) (p_{1\alpha} p_{2\beta} + p_{1\beta} p_{2\alpha}) \right\} \\ & + C_O^{f,W} \left(g_{eG}^V g_{e\Phi}^S + ig_{eG}^A g_{e\Phi}^P \right) g_{\alpha\beta}, \end{aligned} \quad (\text{D.11})$$

$$B_\alpha^{L,\Phi(f,W)} = -\frac{4C_E^{f,W} g_{eG}^V g_{e\Phi}^P m_e^2}{4m_e^2 - q^2} p_{1\alpha} + \left[\frac{2C_E^{f,W} (2m_e^2 - q^2) g_{eG}^V g_{e\Phi}^P}{4m_e^2 - q^2} + 2iC_E^{f,W} g_{eG}^A g_{e\Phi}^S \right] p_{2\alpha}, \quad (\text{D.12})$$

$$B_\alpha^{R,\Phi(f,W)} = - \left[\frac{2C_E^{f,W} (2m_e^2 - q^2) g_{eG}^V g_{e\Phi}^P}{4m_e^2 - q^2} - 2iC_E^{f,W} g_{eG}^A g_{e\Phi}^S \right] p_{1\alpha} + \frac{4C_E^{f,W} g_{eG}^V g_{e\Phi}^P m_e^2}{4m_e^2 - q^2} p_{2\alpha}. \quad (\text{D.13})$$

Note that $A_{\alpha\beta}^{L,\Phi(f,W)}$ and $A_{\alpha\beta}^{R,\Phi(f,W)}$ are symmetric under $\alpha \leftrightarrow \beta$.

D.2 Heavy dark sector

If we expand $F_{\text{DS}}^{\phi_j \eta_a}$ by k^2/M^2 , as in Eq. (3.16), we can easily perform the loop momentum integration. The HDS approximation result is then given by

$$d_e = \sum_{j=1}^{N_E} \sum_{a=2}^{N_O} \left[\sum_f (d_e^f)_{\phi_j \eta_a} + (d_e^W)_{\phi_j \eta_a} \right], \quad (\text{D.14})$$

$$(d_e^{\mathcal{P}})_{\phi_j \eta_a} \simeq \sum_{\Phi=\phi_j, \eta_a} \int_x \int_y \int_z \left\{ a_0^{\phi_j \eta_a}(M^2) \left[\frac{A_{\alpha\beta}^{L,\Phi(\mathcal{P})} + A_{\alpha\beta}^{R,\Phi(\mathcal{P})}}{32\pi^2 \Delta_5(\mathcal{P})^2} g^{\alpha\beta} - \frac{f_5^{L,\Phi(\mathcal{P})} + f_5^{R,\Phi(\mathcal{P})}}{8\pi^2 \Delta_5(\mathcal{P})^3} \right] \right. \\ \left. + \frac{a_1^{\phi_j \eta_a}(M^2)}{M^2} \left[- \frac{3(A_{\alpha\beta}^{L,\Phi(\mathcal{P})} + A_{\alpha\beta}^{R,\Phi(\mathcal{P})})}{32\pi^2 \Delta_5(\mathcal{P})} g^{\alpha\beta} \right. \right. \\ \left. + \frac{\bar{B}^{L,\Phi(\mathcal{P})} \cdot \lambda^L + \bar{B}^{R,\Phi(\mathcal{P})} \cdot \lambda^R}{32\pi^2 \Delta_5(\mathcal{P})^2} + \frac{f_5^{L,\Phi(\mathcal{P})} + f_5^{R,\Phi(\mathcal{P})}}{8\pi^2 \Delta_5(\mathcal{P})^2} \right. \\ \left. \left. + \left(\frac{A_{\alpha\beta}^{L,\Phi(\mathcal{P})} + A_{\alpha\beta}^{R,\Phi(\mathcal{P})}}{32\pi^2 \Delta_5(\mathcal{P})^2} g^{\alpha\beta} - \frac{f_5^{L,\Phi(\mathcal{P})} + f_5^{R,\Phi(\mathcal{P})}}{8\pi^2 \Delta_5(\mathcal{P})^3} \right) C_p^2 m_e^2 \right] \right\}, \quad (\text{D.15})$$

where $\mathcal{P} = f$ or W , $\mathcal{O}(k^4/M^4)$ terms are omitted, and we define

$$\int_z \equiv \int_0^1 dz_1 dz_2 dz_3 dz_4 dz_5 \delta(1 - z_1 - z_2 - z_3 - z_4 - z_5), \quad (\text{D.16})$$

$$\Delta_5(f, W) \equiv \frac{z_1 m_{f,W}^2}{x(1-x)} + z_2 m_{\phi_j}^2 + z_3 m_{\eta_a}^2 + z_4 m_G^2 + z_5^2 m_e^2, \quad (\text{D.17})$$

$$\bar{B}_\alpha^{L,\Phi(f,W)} \equiv -2A_{\alpha\beta}^{L,\Phi(f,W)} (C_q q^\beta - C_p p_2^\beta) + B_\alpha^{L,\Phi(f,W)}, \quad (\text{D.18})$$

$$\bar{B}_\alpha^{R,\Phi(f,W)} \equiv -2A_{\alpha\beta}^{R,\Phi(f,W)} (C_q q^\beta + C_p p_1^\beta) + B_\alpha^{R,\Phi(f,W)}, \quad (\text{D.19})$$

$$f_5^{L,\Phi(f,W)} \equiv A_{\alpha\beta}^{L,\Phi(f,W)} (C_q q^\alpha - C_p p_2^\alpha) (C_q q^\beta - C_p p_2^\beta) - B_\alpha^{L,\Phi(f,W)} (C_q q^\alpha - C_p p_2^\alpha), \quad (\text{D.20})$$

$$f_5^{R,\Phi(f,W)} \equiv A_{\alpha\beta}^{R,\Phi(f,W)} (C_q q^\alpha + C_p p_1^\alpha) (C_q q^\beta + C_p p_1^\beta) - B_\alpha^{R,\Phi(f,W)} (C_q q^\alpha + C_p p_1^\alpha), \quad (\text{D.21})$$

$$\lambda^L \equiv 2(1 - C_q)q + 2C_p p_2, \quad (\text{D.22})$$

$$\lambda^R \equiv 2(1 - C_q)q - 2C_p p_1, \quad (\text{D.23})$$

$$C_q = \frac{y}{1-x} z_1 + z_2 + z_3, \quad C_p = (1 - z_1 - z_2 - z_3 - z_4). \quad (\text{D.24})$$

Here, C_q and C_p correspond to the momentum shift originated from the $k \cdot p_i$ and $k \cdot q$ terms in the denominator,

$$k \rightarrow \tilde{k} = \begin{cases} k + C_q q - C_p p_2 & \text{for Eq. (D.1)} \\ k + C_q q + C_p p_1 & \text{for Eq. (D.7)} \end{cases}. \quad (\text{D.25})$$

Note that due to $q^2 = 0$ which leads to $p_{1,2} \cdot q = 0$, we have $\lambda^L \cdot \lambda^L = \lambda^R \cdot \lambda^R = 4C_p^2 m_e^2$. For the diagram with $\Gamma^{\mu\nu}$ for the inner loop, each term can be calculated as

$$(A_{\alpha\beta}^{L,\Phi(f,W)} + A_{\alpha\beta}^{R,\Phi(f,W)})g^{\alpha\beta} = -4g_e^V \left(C_E^{f,W} g_e^P - C_O^{f,W} g_e^S \right), \quad (\text{D.26})$$

$$\bar{B}^{L,\Phi(f,W)} \cdot \lambda^L + \bar{B}^{R,\Phi(f,W)} \cdot \lambda^R = -8C_p^2 C_E^{f,W} g_e^V g_e^P m_e^2, \quad (\text{D.27})$$

$$f_5^{L,\Phi(f,W)} + f_5^{R,\Phi(f,W)} = -2C_p^2 C_E^{f,W} g_e^V g_e^P m_e^2. \quad (\text{D.28})$$

It should be emphasized that the effects of $k \cdot p_i$ and $k \cdot q$ in the denominator of Eqs. (D.1) and (D.7) appear in the final result as sub-dominant terms: once we set $C_{q,p} = 0$ which means no momentum shift for k , Eq. (D.15) becomes the leading results in Eq. (3.17). This can be understood by the fact that Eqs. (D.27) and (D.28) and the last term in Eq. (D.15) become zero. This feature remains even for the general result without the HDS approximation shown in Eq. (3.13).

D.3 Decomposed expressions for the electron EDM

In Eq. (4.28), we define two parts of contributions to the electron EDM: $F_{\text{DS}}^{\phi_j \eta_a}$ and the renormalization part. Here, the explicit form of each contribution is shown.

Let us start with the case of a general dark sector. In our setup, we have effective mixing between CP-even (ϕ_j) and CP-odd (η_a) scalars via a dark sector CP violation, denoted as $F_{\text{DS}}^{\phi_j \eta_a}$. If $F_{\text{DS}}^{\phi_j \eta_a}$ has a UV divergent part, as in the two benchmark models, the divergence needs to be treated appropriately. In the on-shell subtraction scheme, we can remove it and obtain a renormalized one:

$$\hat{\Sigma}_{\phi_j \eta_a} = F_{\text{DS}}^{\phi_j \eta_a} + \delta F_{\text{DS}}^{\phi_j \eta_a}, \quad (\text{D.29})$$

where $\delta F_{\text{DS}}^{\phi_j \eta_a}$ corresponds to the term induced by renormalization. Then, the UV divergence is canceled, and hence, we find a finite prediction,

$$\hat{\Sigma}_{\phi_j \eta_a} = \tilde{F}_{\text{DS}}^{\phi_j \eta_a} + \tilde{\delta F}_{\text{DS}}^{\phi_j \eta_a}. \quad (\text{D.30})$$

Here, $\tilde{F}_{\text{DS}}^{\phi_j \eta_a}$ and $\tilde{\delta F}_{\text{DS}}^{\phi_j \eta_a}$ do not have any divergent part. Note that they also do not have any constant term associated with the momentum passing through this effective mixing. Using this notation, we can now find the explicit formulas for $d_e^{\text{Org.,Ren.}}$ as

$$d_e^{\text{Org.}} = \sum_{j=1}^{N_E} \sum_{a=2}^{N_O} \int_x \int_y \int_k \frac{\tilde{F}_{\text{DS}}^{\phi_j \eta_a}((k+q)^2, M^2)}{(k^2 - \Delta)(k^2 - m_G^2)(k^2 + 2k \cdot q - m_{\phi_j}^2)(k^2 + 2k \cdot q - m_{\eta_a}^2)}$$

$$\times \sum_{\Phi=\phi_j, \eta_a} \left(\frac{A_{\alpha\beta}^{L,\Phi} k^\alpha k^\beta + B_\alpha^{L,\Phi} k^\alpha}{k^2 - 2k \cdot p_2} + \frac{A_{\alpha\beta}^{R,\Phi} k^\alpha k^\beta + B_\alpha^{R,\Phi} k^\alpha}{k^2 + 2k \cdot p_1} \right), \quad (\text{D.31})$$

$$d_e^{\text{Ren.}} = \sum_{j=1}^{N_E} \sum_{a=2}^{N_O} \int_x \int_y \int_k \frac{\widetilde{\delta F}_{\text{DS}}^{\phi_j \eta_a}((k+q)^2, M^2)}{(k^2 - \Delta)(k^2 - m_G^2)(k^2 + 2k \cdot q - m_{\phi_j}^2)(k^2 + 2k \cdot q - m_{\eta_a}^2)} \\ \times \sum_{\Phi=\phi_j, \eta_a} \left(\frac{A_{\alpha\beta}^{L,\Phi} k^\alpha k^\beta + B_\alpha^{L,\Phi} k^\alpha}{k^2 - 2k \cdot p_2} + \frac{A_{\alpha\beta}^{R,\Phi} k^\alpha k^\beta + B_\alpha^{R,\Phi} k^\alpha}{k^2 + 2k \cdot p_1} \right), \quad (\text{D.32})$$

where we omit the superscript f and W from the general result in Eq. (3.13) for simplicity. Note that for $d_e^{\text{Ren.}}$, a further calculation can be done as in the case of the HDS limit in section 3.4.1, because the on-shell subtraction scheme gives additional terms which are proportional to the squared momentum and constant (see Eqs. (4.18), (4.19) and (4.46)). For the HDS approximation, we expand $\widetilde{F}_{\text{DS}}^{\phi_j \eta_a}((k+q)^2, M^2)$ and $\widetilde{\delta F}_{\text{DS}}^{\phi_j \eta_a}((k+q)^2, M^2)$ with respect to k^2/M^2 .

For the scalar dark sector model, we have

$$\widetilde{F}_{\text{DS}}^{hA}(k^2) = -\frac{v_{\text{SM}}^2}{64\pi^2} \lambda_{12S}^- s_{2\theta_s} \left[\lambda_{12S}^+ c_{\alpha+\beta} c_{2\theta_s} \left(\text{DiscB}(k^2, m_{\varphi_1}, m_{\varphi_1}) + \text{DiscB}(k^2, m_{\varphi_2}, m_{\varphi_2}) \right. \right. \\ \left. \left. - 2\text{DiscB}(k^2, m_{\varphi_1}, m_{\varphi_2}) + \frac{m_{\varphi_1}^2 - m_{\varphi_2}^2}{k^2} \ln \frac{m_{\varphi_1}^2}{m_{\varphi_2}^2} \right) \right. \\ \left. + \lambda_{hS} \left(\text{DiscB}(k^2, m_{\varphi_1}, m_{\varphi_1}) - \text{DiscB}(k^2, m_{\varphi_2}, m_{\varphi_2}) \right) \right], \quad (\text{D.33})$$

$$\widetilde{\delta F}_{\text{DS}}^{hA}(k^2) = -\frac{v_{\text{SM}}^2}{64\pi^2} \lambda_{12S}^- s_{2\theta_s} \left[\frac{k^2 - m_A^2}{m_A^2 - m_h^2} \left(\lambda_{12S}^+ c_{\alpha+\beta} c_{2\theta_s} \overline{\mathcal{F}}_1(m_h, m_{\varphi_1}, m_{\varphi_2}) \right. \right. \\ \left. \left. + \lambda_{hS} \mathcal{F}_2(m_h, m_{\varphi_1}, m_{\varphi_2}) \right) \right. \\ \left. + \frac{m_h^2 - k^2}{m_A^2 - m_h^2} \left(\lambda_{12S}^+ c_{\alpha+\beta} c_{2\theta_s} \overline{\mathcal{F}}_1(m_A, m_{\varphi_1}, m_{\varphi_2}) \right. \right. \\ \left. \left. + \lambda_{hS} \mathcal{F}_2(m_A, m_{\varphi_1}, m_{\varphi_2}) \right) \right], \quad (\text{D.34})$$

$$\widetilde{F}_{\text{DS}}^{HA}(k^2) = -\frac{v_{\text{SM}}^2}{64\pi^2} \lambda_{12S}^- s_{2\theta_s} \left[\lambda_{12S}^+ s_{\alpha+\beta} c_{2\theta_s} \left(\text{DiscB}(k^2, m_{\varphi_1}, m_{\varphi_1}) + \text{DiscB}(k^2, m_{\varphi_2}, m_{\varphi_2}) \right. \right. \\ \left. \left. - 2\text{DiscB}(k^2, m_{\varphi_1}, m_{\varphi_2}) + \frac{m_{\varphi_1}^2 - m_{\varphi_2}^2}{k^2} \ln \frac{m_{\varphi_1}^2}{m_{\varphi_2}^2} \right) \right. \\ \left. + \lambda_{HS} \left(\text{DiscB}(k^2, m_{\varphi_1}, m_{\varphi_1}) - \text{DiscB}(k^2, m_{\varphi_2}, m_{\varphi_2}) \right) \right], \quad (\text{D.35})$$

$$\begin{aligned} \widetilde{\delta F}_{\text{DS}}^{HA}(k^2) = & -\frac{v_{\text{SM}}^2}{64\pi^2} \lambda_{12S}^- s_{2\theta_s} \left[\frac{k^2 - m_A^2}{m_A^2 - m_H^2} \left(\lambda_{12S}^+ s_{\alpha+\beta} c_{2\theta_s} \overline{\mathcal{F}}_1(m_H, m_{\varphi_1}, m_{\varphi_2}) \right. \right. \\ & \left. \left. + \lambda_{HS} \mathcal{F}_2(m_H, m_{\varphi_1}, m_{\varphi_2}) \right) \right. \\ & \left. + \frac{m_H^2 - k^2}{m_A^2 - m_H^2} \left(\lambda_{12S}^+ s_{\alpha+\beta} c_{2\theta_s} \overline{\mathcal{F}}_1(m_A, m_{\varphi_1}, m_{\varphi_2}) \right. \right. \\ & \left. \left. + \lambda_{hS} \mathcal{F}_2(m_A, m_{\varphi_1}, m_{\varphi_2}) \right) \right], \end{aligned} \quad (\text{D.36})$$

$$(\text{D.37})$$

where

$$\overline{\mathcal{F}}_1(m, m_{\varphi_1}, m_{\varphi_2}) \equiv \mathcal{F}_1(m, m_{\varphi_1}, m_{\varphi_2}) + \frac{m_{\varphi_1}^2 - m_{\varphi_2}^2}{m^2} \ln \frac{m_{\varphi_1}^2}{m_{\varphi_2}^2}, \quad (\text{D.38})$$

and $\mathcal{F}_1(m, m_{\varphi_1}, m_{\varphi_2})$ and $\mathcal{F}_2(m, m_{\varphi_1}, m_{\varphi_2})$ are given in Eqs. (4.25) and (4.26), respectively. For the HDS approximation, we can obtain the expressions by expanding each of them in the heavy $m_{\varphi_{1,2}}$ limit as

$$\begin{aligned} \widetilde{F}_{\text{DS}}^{hA,\text{HDS}}(k^2) = & -\frac{v_{\text{SM}}^2}{64\pi^2} \lambda_{12S}^- s_{2\theta_s} \left[\lambda_{12S}^+ c_{\alpha+\beta} c_{2\theta_s} \left(-2 + \frac{m_{\varphi_1}^2 + m_{\varphi_2}^2}{m_{\varphi_1}^2 - m_{\varphi_2}^2} \ln \frac{m_{\varphi_1}^2}{m_{\varphi_2}^2} \right. \right. \\ & \left. \left. + k^2 \left\{ \frac{(m_{\varphi_1}^2 + m_{\varphi_2}^2)(m_{\varphi_1}^4 - 8m_{\varphi_1}^2 m_{\varphi_2}^2 + m_{\varphi_2}^4)}{6m_{\varphi_1}^2 m_{\varphi_2}^2 (m_{\varphi_1}^2 - m_{\varphi_2}^2)^2} \right. \right. \right. \\ & \left. \left. \left. + \frac{2m_{\varphi_1}^2 m_{\varphi_2}^2}{(m_{\varphi_1}^2 - m_{\varphi_2}^2)^3} \ln \frac{m_{\varphi_1}^2}{m_{\varphi_2}^2} \right\} \right) - \lambda_{hS} \frac{m_{\varphi_1}^2 - m_{\varphi_2}^2}{6m_{\varphi_1}^2 m_{\varphi_2}^2} k^2 \right], \end{aligned} \quad (\text{D.39})$$

$$\begin{aligned} \widetilde{F}_{\text{DS}}^{HA,\text{HDS}}(k^2) = & -\frac{v_{\text{SM}}^2}{64\pi^2} \lambda_{12S}^- s_{2\theta_s} \left[\lambda_{12S}^+ s_{\alpha+\beta} c_{2\theta_s} \left(-2 + \frac{m_{\varphi_1}^2 + m_{\varphi_2}^2}{m_{\varphi_1}^2 - m_{\varphi_2}^2} \ln \frac{m_{\varphi_1}^2}{m_{\varphi_2}^2} \right. \right. \\ & \left. \left. + k^2 \left\{ \frac{(m_{\varphi_1}^2 + m_{\varphi_2}^2)(m_{\varphi_1}^4 - 8m_{\varphi_1}^2 m_{\varphi_2}^2 + m_{\varphi_2}^4)}{6m_{\varphi_1}^2 m_{\varphi_2}^2 (m_{\varphi_1}^2 - m_{\varphi_2}^2)^2} \right. \right. \right. \\ & \left. \left. \left. + \frac{2m_{\varphi_1}^2 m_{\varphi_2}^2}{(m_{\varphi_1}^2 - m_{\varphi_2}^2)^3} \ln \frac{m_{\varphi_1}^2}{m_{\varphi_2}^2} \right\} \right) - \lambda_{HS} \frac{m_{\varphi_1}^2 - m_{\varphi_2}^2}{6m_{\varphi_1}^2 m_{\varphi_2}^2} k^2 \right]. \end{aligned} \quad (\text{D.40})$$

Here, we omit $\mathcal{O}(k^4/m_{\varphi_i}^4)$ terms, and $\widetilde{\delta F}_{\text{DS}}^{hA,\text{HDS}}(k^2)$ and $\widetilde{\delta F}_{\text{DS}}^{HA,\text{HDS}}(k^2)$ are the same as $\widetilde{\delta F}_{\text{DS}}^{hA}(k^2)$ and $\widetilde{\delta F}_{\text{DS}}^{HA}(k^2)$.

For the fermion dark sector model, we find

$$\widetilde{F}_{\text{DS}}^{\phi_j \eta^a}(k^2) = \frac{y_\psi^R y_\psi^I}{8\pi^2} m_\psi^2 (R_E)_{3j} (R_O)_{3a} \text{DiscB}(k^2, m_\psi, m_\psi), \quad (\text{D.41})$$

$$\widetilde{\delta F}_{\text{DS}}^{\phi_j \eta_a}(k^2) = \frac{y_\psi^R y_\psi^I}{8\pi^2} m_\psi^2 (R_E)_{3j} (R_O)_{3a} \left[\frac{m_{\eta_a}^2 - k^2}{m_{\phi_j}^2 - m_{\eta_a}^2} \text{Re}\{\text{DiscB}(m_{\phi_j}^2, m_\psi, m_\psi)\} \right. \\ \left. + \frac{k^2 - m_{\phi_j}^2}{m_{\phi_j}^2 - m_{\eta_a}^2} \text{Re}\{\text{DiscB}(m_{\eta_a}^2, m_\psi, m_\psi)\} \right]. \quad (\text{D.42})$$

For the HDS approximation, they are

$$\widetilde{F}_{\text{DS}}^{\phi_j \eta_a, \text{HDS}}(k^2) = \frac{y_\psi^R y_\psi^I}{8\pi^2} m_\psi^2 (R_E)_{3j} (R_O)_{3a} \left(-2 + \frac{k^2}{6m_\psi^2} \right), \quad (\text{D.43})$$

and $\widetilde{\delta F}_{\text{DS}}^{\phi_j \eta_a, \text{HDS}}(k^2)$ unchanged from $\widetilde{\delta F}_{\text{DS}}^{\phi_j \eta_a}(k^2)$.

References

- [1] ATLAS collaboration, *Observation of a new particle in the search for the Standard Model Higgs boson with the ATLAS detector at the LHC*, *Phys. Lett. B* **716** (2012) 1 [[1207.7214](#)].
- [2] CMS collaboration, *Observation of a New Boson at a Mass of 125 GeV with the CMS Experiment at the LHC*, *Phys. Lett. B* **716** (2012) 30 [[1207.7235](#)].
- [3] T. D. Lee, *A Theory of Spontaneous T Violation*, *Phys. Rev. D* **8** (1973) 1226.
- [4] G. C. Branco, P. M. Ferreira, L. Lavoura, M. N. Rebelo, M. Sher and J. P. Silva, *Theory and phenomenology of two-Higgs-doublet models*, *Phys. Rept.* **516** (2012) 1 [[1106.0034](#)].
- [5] K. Inoue, A. Kakuto, H. Komatsu and S. Takeshita, *Low Energy Parameters and Particle Masses in a Supersymmetric Grand Unified Model*, *Progress of Theoretical Physics* **67** (1982) 1889 [<https://academic.oup.com/ptp/article-pdf/67/6/1889/5333146/67-6-1889.pdf>].
- [6] P. Fayet, *Supergauge invariant extension of the higgs mechanism and a model for the electron and its neutrino*, *Nuclear Physics B* **90** (1975) 104.
- [7] J. F. Gunion and H. E. Haber, *Higgs Bosons in Supersymmetric Models. 1.*, *Nucl. Phys. B* **272** (1986) 1.
- [8] R. A. Flores and M. Sher, *Higgs masses in the standard, multi-higgs and supersymmetric models*, *Annals of Physics* **148** (1983) 95.
- [9] N. G. Deshpande and E. Ma, *Pattern of Symmetry Breaking with Two Higgs Doublets*, *Phys. Rev. D* **18** (1978) 2574.

- [10] L. Lopez Honorez, E. Nezri, J. F. Oliver and M. H. G. Tytgat, *The Inert Doublet Model: An Archetype for Dark Matter*, *JCAP* **02** (2007) 028 [[hep-ph/0612275](#)].
- [11] E. M. Dolle and S. Su, *The Inert Dark Matter*, *Phys. Rev. D* **80** (2009) 055012 [[0906.1609](#)].
- [12] L. Lopez Honorez and C. E. Yaguna, *The inert doublet model of dark matter revisited*, *JHEP* **09** (2010) 046 [[1003.3125](#)].
- [13] N. Blinov, J. Kozaczuk, D. E. Morrissey and A. de la Puente, *Compressing the Inert Doublet Model*, *Phys. Rev. D* **93** (2016) 035020 [[1510.08069](#)].
- [14] M. Krawczyk, N. Darvishi and D. Sokolowska, *The Inert Doublet Model and its extensions*, *Acta Phys. Polon. B* **47** (2016) 183 [[1512.06437](#)].
- [15] M. Carena, M. Quirós and Y. Zhang, *Electroweak Baryogenesis from Dark-Sector CP Violation*, *Phys. Rev. Lett.* **122** (2019) 201802 [[1811.09719](#)].
- [16] M. Carena, M. Quirós and Y. Zhang, *Dark CP violation and gauged lepton or baryon number for electroweak baryogenesis*, *Phys. Rev. D* **101** (2020) 055014 [[1908.04818](#)].
- [17] ACME collaboration, *Improved limit on the electric dipole moment of the electron*, *Nature* **562** (2018) 355.
- [18] T. S. Roussy et al., *An improved bound on the electron's electric dipole moment*, *Science* **381** (2023) adg4084 [[2212.11841](#)].
- [19] L. Caldwell et al., *Systematic and statistical uncertainty evaluation of the $HfF+$ electron electric dipole moment experiment*, *Phys. Rev. A* **108** (2023) 012804 [[2212.11837](#)].
- [20] S. Okawa, M. Pospelov and A. Ritz, *Electric Dipole Moments From Dark Sectors*, *Phys. Rev. D* **100** (2019) 075017 [[1905.05219](#)].
- [21] T.-K. Chen, C.-W. Chiang and I. Low, *Simple model of dark matter and CP violation*, *Phys. Rev. D* **105** (2022) 075025 [[2202.02954](#)].
- [22] C. H. de Lima, B. Keeshan, H. E. Logan and Y. Zhang, *Probing dark sector CP violation with electric dipole moments and colliders*, *Phys. Rev. D* **103** (2021) 115034 [[2010.06441](#)].
- [23] D. Azevedo, P. M. Ferreira, M. M. Muhlleitner, S. Patel, R. Santos and J. Wittbrodt, *CP in the dark*, *JHEP* **11** (2018) 091 [[1807.10322](#)].

- [24] D. Egana-Ugrinovic and S. Thomas, *Higgs Boson Contributions to the Electron Electric Dipole Moment*, [1810.08631](#).
- [25] E. J. Chun, J. Kim and T. Mondal, *Electron EDM and Muon anomalous magnetic moment in Two-Higgs-Doublet Models*, *JHEP* **12** (2019) 068 [[1906.00612](#)].
- [26] K. Cheung, A. Jueid, Y.-N. Mao and S. Moretti, *Two-Higgs-doublet model with soft CP violation confronting electric dipole moments and colliders*, *Phys. Rev. D* **102** (2020) 075029 [[2003.04178](#)].
- [27] S. Kanemura, M. Kubota and K. Yagyu, *Aligned CP-violating Higgs sector canceling the electric dipole moment*, *JHEP* **08** (2020) 026 [[2004.03943](#)].
- [28] N. Chen, T. Li, Z. Teng and Y. Wu, *Collapsing domain walls in the two-Higgs-doublet model and deep insights from the EDM*, *JHEP* **10** (2020) 081 [[2006.06913](#)].
- [29] I. Low, N. R. Shah and X.-P. Wang, *Higgs alignment and novel CP-violating observables in two-Higgs-doublet models*, *Phys. Rev. D* **105** (2022) 035009 [[2012.00773](#)].
- [30] S. Kanemura, M. Kubota and K. Yagyu, *Testing aligned CP-violating Higgs sector at future lepton colliders*, *JHEP* **04** (2021) 144 [[2101.03702](#)].
- [31] M. Frank, E. G. Fuakye and M. Toharia, *Restricting the parameter space of type-II two-Higgs-doublet models with CP violation*, *Phys. Rev. D* **106** (2022) 035010 [[2112.14295](#)].
- [32] S. Kanemura, K. Katayama, T. Mondal and K. Yagyu, *Multi-photon signatures as a probe of CP-violation in extended Higgs sectors*, [2308.01772](#).
- [33] S. L. Glashow and S. Weinberg, *Natural Conservation Laws for Neutral Currents*, *Phys. Rev. D* **15** (1977) 1958.
- [34] A. Djouadi, *The Anatomy of electro-weak symmetry breaking. II. The Higgs bosons in the minimal supersymmetric model*, *Phys. Rept.* **459** (2008) 1 [[hep-ph/0503173](#)].
- [35] MUON (G-2) collaboration, *An Improved Limit on the Muon Electric Dipole Moment*, *Phys. Rev. D* **80** (2009) 052008 [[0811.1207](#)].
- [36] C. Abel et al., *Measurement of the Permanent Electric Dipole Moment of the Neutron*, *Phys. Rev. Lett.* **124** (2020) 081803 [[2001.11966](#)].

- [37] Y. Nakai and M. Reece, *Electric Dipole Moments in Natural Supersymmetry*, *JHEP* **08** (2017) 031 [[1612.08090](#)].
- [38] C. Cesarotti, Q. Lu, Y. Nakai, A. Parikh and M. Reece, *Interpreting the Electron EDM Constraint*, *JHEP* **05** (2019) 059 [[1810.07736](#)].
- [39] M. Pospelov and A. Ritz, *Electric dipole moments as probes of new physics*, *Annals Phys.* **318** (2005) 119 [[hep-ph/0504231](#)].
- [40] J. Engel, M. J. Ramsey-Musolf and U. van Kolck, *Electric Dipole Moments of Nucleons, Nuclei, and Atoms: The Standard Model and Beyond*, *Prog. Part. Nucl. Phys.* **71** (2013) 21 [[1303.2371](#)].
- [41] T. Chupp, P. Fierlinger, M. Ramsey-Musolf and J. Singh, *Electric dipole moments of atoms, molecules, nuclei, and particles*, *Rev. Mod. Phys.* **91** (2019) 015001 [[1710.02504](#)].
- [42] B. Graner, Y. Chen, E. G. Lindahl and B. R. Heckel, *Reduced Limit on the Permanent Electric Dipole Moment of Hg199*, *Phys. Rev. Lett.* **116** (2016) 161601 [[1601.04339](#)].
- [43] J. R. Ellis, J. S. Lee and A. Pilaftsis, *Electric Dipole Moments in the MSSM Reloaded*, *JHEP* **10** (2008) 049 [[0808.1819](#)].
- [44] M. Jung and A. Pich, *Electric Dipole Moments in Two-Higgs-Doublet Models*, *JHEP* **04** (2014) 076 [[1308.6283](#)].
- [45] S. M. Barr and A. Zee, *Electric dipole moment of the electron and of the neutron*, *Phys. Rev. Lett.* **65** (1990) 21.
- [46] P. Junnarkar and A. Walker-Loud, *Scalar strange content of the nucleon from lattice QCD*, *Phys. Rev. D* **87** (2013) 114510 [[1301.1114](#)].
- [47] T. Abe, J. Hisano, T. Kitahara and K. Tobioka, *Gauge invariant Barr-Zee type contributions to fermionic EDMs in the two-Higgs doublet models*, *JHEP* **01** (2014) 106 [[1311.4704](#)].
- [48] W. Altmannshofer, S. Gori, N. Hamer and H. H. Patel, *Electron EDM in the complex two-Higgs doublet model*, *Phys. Rev. D* **102** (2020) 115042 [[2009.01258](#)].
- [49] S. Inoue, M. J. Ramsey-Musolf and Y. Zhang, *CP-violating phenomenology of flavor conserving two Higgs doublet models*, *Phys. Rev. D* **89** (2014) 115023 [[1403.4257](#)].

- [50] S. Inoue, G. Ovanessian and M. J. Ramsey-Musolf, *Two-Step Electroweak Baryogenesis*, *Phys. Rev. D* **93** (2016) 015013 [[1508.05404](#)].
- [51] L. Altenkamp, S. Dittmaier and H. Rzehak, *Renormalization schemes for the Two-Higgs-Doublet Model and applications to $h \rightarrow WW/ZZ \rightarrow 4$ fermions*, *JHEP* **09** (2017) 134 [[1704.02645](#)].
- [52] A. Denner, *Techniques for calculation of electroweak radiative corrections at the one loop level and results for W physics at LEP-200*, *Fortsch. Phys.* **41** (1993) 307 [[0709.1075](#)].
- [53] A. Pilaftsis, *CP odd tadpole renormalization of Higgs scalar - pseudoscalar mixing*, *Phys. Rev. D* **58** (1998) 096010 [[hep-ph/9803297](#)].
- [54] A. Pilaftsis, *Higgs scalar - pseudoscalar mixing in the minimal supersymmetric standard model*, *Phys. Lett. B* **435** (1998) 88 [[hep-ph/9805373](#)].
- [55] A. Pilaftsis and C. E. M. Wagner, *Higgs bosons in the minimal supersymmetric standard model with explicit CP violation*, *Nucl. Phys. B* **553** (1999) 3 [[hep-ph/9902371](#)].
- [56] M. Krause, R. Lorenz, M. Muhlleitner, R. Santos and H. Ziesche, *Gauge-independent Renormalization of the 2-Higgs-Doublet Model*, *JHEP* **09** (2016) 143 [[1605.04853](#)].
- [57] A. Denner, L. Jenniches, J.-N. Lang and C. Sturm, *Gauge-independent \overline{MS} renormalization in the 2HDM*, *JHEP* **09** (2016) 115 [[1607.07352](#)].
- [58] A. Denner, S. Dittmaier and J.-N. Lang, *Renormalization of mixing angles*, *JHEP* **11** (2018) 104 [[1808.03466](#)].
- [59] A. Denner and S. Dittmaier, *Electroweak Radiative Corrections for Collider Physics*, *Phys. Rept.* **864** (2020) 1 [[1912.06823](#)].
- [60] D. Fontes and J. C. Romão, *Renormalization of the C2HDM with FeynMaster 2*, *JHEP* **06** (2021) 016 [[2103.06281](#)].
- [61] J. Fleischer and F. Jegerlehner, *Radiative Corrections to Higgs Decays in the Extended Weinberg-Salam Model*, *Phys. Rev. D* **23** (1981) 2001.
- [62] T. Biekötter and M. Pierre, *Higgs-boson visible and invisible constraints on hidden sectors*, *Eur. Phys. J. C* **82** (2022) 1026 [[2208.05505](#)].
- [63] R. Alarcon et al., *Electric dipole moments and the search for new physics*, in *Snowmass 2021*, 3, 2022, [2203.08103](#).